High performance computing of earthquake dynamic rupture scenarios on natural fault zones with SeisSol

Alice-Agnes Gabriel

SCEC Rupture Dynamics Code Validation Workshop
23.03.2015

In collaboration with:

The SeisSol Core Team

LMU LUDWIG-MAXIMILIANS-UNIVERSITÄT MÜNCHEN

Stephanie Wollherr

Thomas Ulrich

Alice Gabriel

… starting in June '15

Betsy Madden

… now at Munich Re

Christian Pelties

TECHNISCHE UNIVERSITÄT MÜNCHEN

Alexander Breuer

Sebastian Rettenberger

Michael Bader

intel

Alexander Heinecke

SeisSol – an ADER-DG based software package

- Arbitrary high-order derivative Discontinuous Galerkin (**ADER-DG**) scheme
- Target applications:
  - Seismic wave propagation
  - Exploration industry
  - Dynamic rupture earthquake scenarios
- **complex geometries** (topography, interfaces)
  - **heterogeneous media** (acoustic, elastic, viscoelastic, anisotropic)
    - **multi-physics** (rupture dynamics)

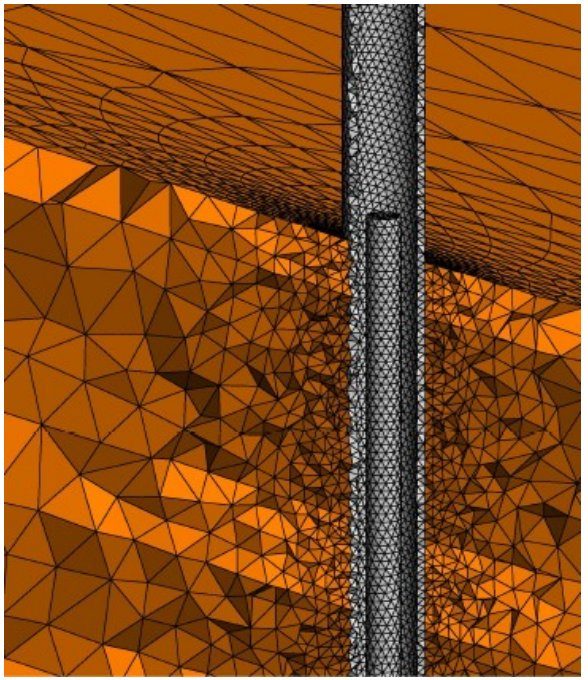

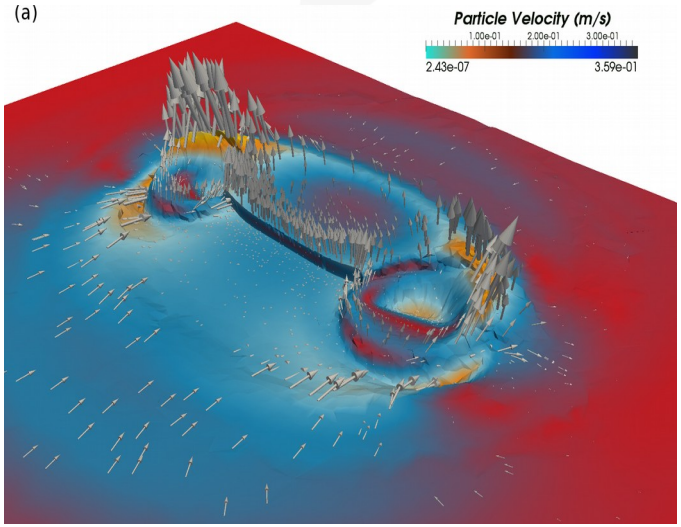

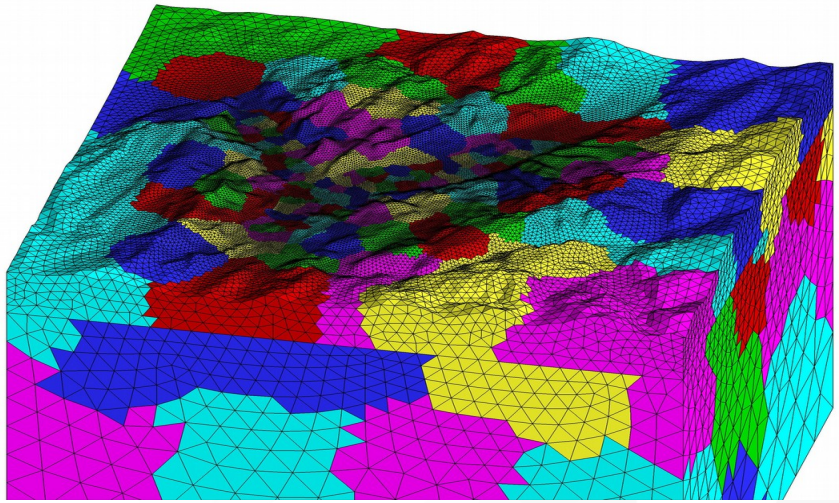

SeisSol – an ADER-DG based software package

- Arbitrary high-order derivative Discontinuous Galerkin (**ADER-DG**) scheme
- Target applications:
  - Seismic wave propagation
  - Exploration industry
  - Dynamic rupture earthquake scenarios

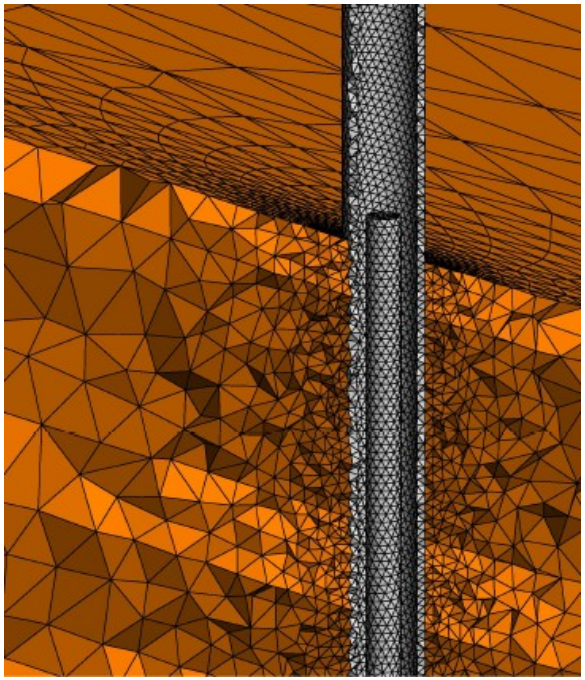

- **complex geometries** (topography, interfaces)
  - **heterogeneous media** (acoustic, elastic, viscoelastic, anisotropic)
    - **multi-physics** (rupture dynamics)

- **But:** computationally expensive and non-trivial to implement

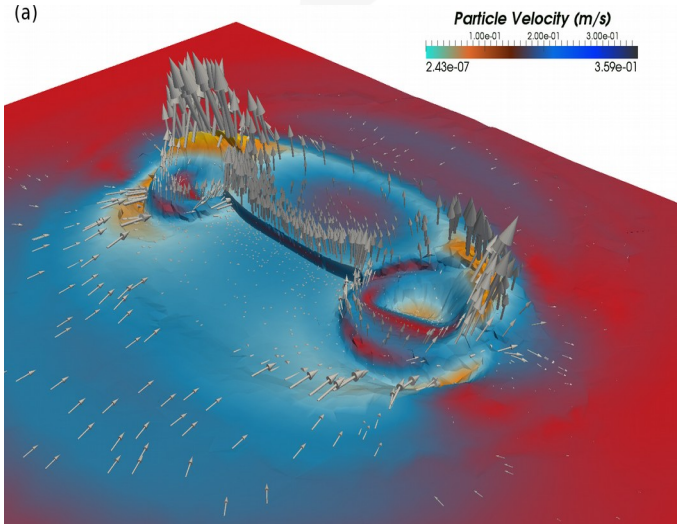

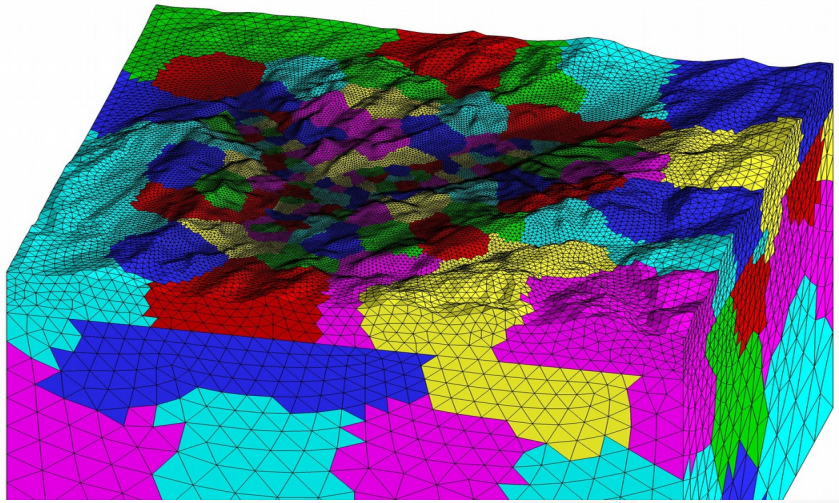

SeisSol – an ADER-DG based software package

- **ADER**: high-order time integration + **DG**: high-order space discretization
- Elastic wave equation in **velocity stress** formulation (linear hyperbolic system)
- DG discretization with orthogonal basis functions (**modal**)
- **Exact Riemann-Solver** computes the upwind flux = state at the element interfaces
- **Locality** of the computations: only neighboring elements are required to exchange data

$$\frac{\partial Q_p}{\partial t} + A_{pq}\frac{\partial Q_q}{\partial x} + B_{pq}\frac{\partial Q_q}{\partial y} + C_{pq}\frac{\partial Q_q}{\partial z} = S_p$$

$$Q = (\sigma_{xx}, \sigma_{yy}, \sigma_{zz}, \sigma_{xy}, \sigma_{yz}, \sigma_{xz}, u, v, w)^T$$

PDE

$$\tilde{K}^{\xi}\left(\mathcal{J}_k^{n,n+1}\right) A_k^{\star} + \tilde{K}^{\eta}\left(\mathcal{J}_k^{n,n+1}\right) B_k^{\star} + \tilde{K}^{\zeta}\left(\mathcal{J}_k^{n,n+1}\right) C_k^{\star}$$

DG discrete form

SeisSol – an ADER-DG based software package

- **ADER**: high-order time integration + **DG**: high-order space discretization
- Elastic wave equation in **velocity stress** formulation (linear hyperbolic system)
- DG discretization with orthogonal basis functions (**modal**)
- **Exact Riemann-Solver** computes the upwind flux = state at the element interfaces
- **Locality** of the computations: only neighboring elements are required to exchange data

$$\frac{\partial Q_p}{\partial t} + A_{pq}\frac{\partial Q_q}{\partial x} + B_{pq}\frac{\partial Q_q}{\partial y} + C_{pq}\frac{\partial Q_q}{\partial z} = S_p$$

$$Q = (\sigma_{xx}, \sigma_{yy}, \sigma_{zz}, \sigma_{xy}, \sigma_{yz}, \sigma_{xz}, u, v, w)^T$$

PDE

$$\tilde{K}^{\xi}\left(\mathcal{J}_k^{n,n+1}\right) A_k^{\star} + \tilde{K}^{\eta}\left(\mathcal{J}_k^{n,n+1}\right) B_k^{\star} + \tilde{K}^{\zeta}\left(\mathcal{J}_k^{n,n+1}\right) C_k^{\star}$$

DG discrete form

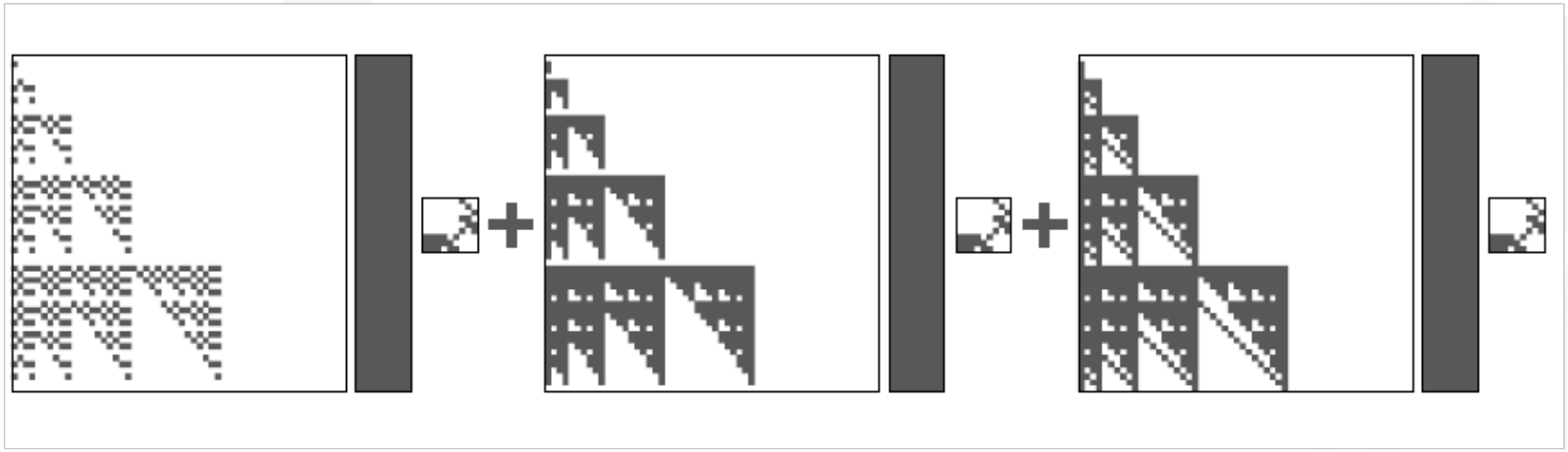

DG operators

→ Very small dense and sparse linear algebra operations per element

(~75% of runtime consumption)

Optimization of SeisSol – Wave propagation on petascale supercomputers

- **Highly optimized compute kernels** for sparse-dense matrix products generated by off-line code generator

  → hardware specific full “unrolling” and vectorization of all element operations

- Optimization of **parallel I/O**

  → customized parallel mesh format and mesher

  → largest mesh: > 3.5 billion cells

- **Speed-up** of ~5-10, 90% parallel efficiency, 45% of peak theoretical performance

  → For comparison:

  - AWP 2010: 5% peak performance on Titan (GPU powered)
  - SpecFEM 2013: 15% peak performance on 700k BlueWaters cores (GPU powered)
  - *Note that peak performance implies nothing about time-to-solution*

(Breuer et al., Prace Award, ISC14)

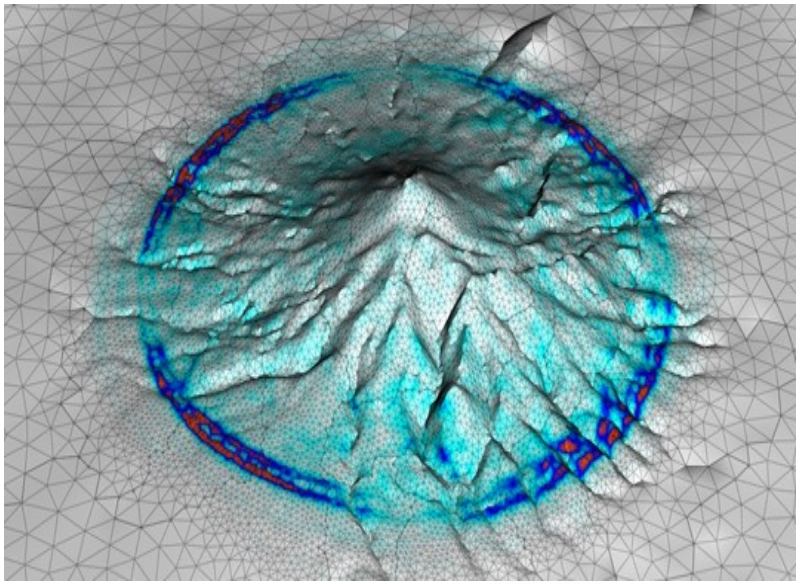

Wave field of a point source interacting with the topography of Mount Merap Volcano

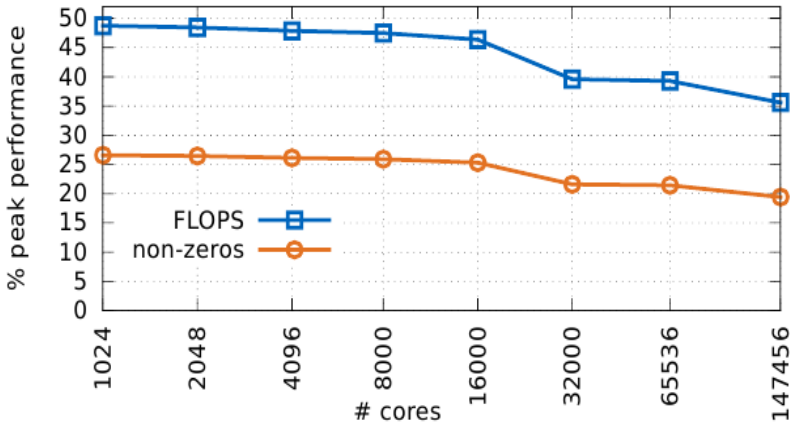

Fig. 4. Strong scaling of the Mount Merapi benchmark with 99,831,401 tetrahedrons using approximation order $\mathcal{O} = 6$. Shown are hardware FLOPS (blue) and non-zero operations (orange).

SeisSol for Rupture Dynamics

- Dynamic rupture boundary condition (temporal numerical flux condition) causes **no artificial spurious oscillations**
- **Verified** for numerically challenging fault geometries and rheologies (SCEC benchmarks)
- → branching and dipping fault systems, heterogeneous background stresses, bi-material faults, off-fault plastic deformation and rate-and-state friction

Two triangle-based polynomial representations of shear stress discontinuous at the fault interface. Spontaneous rupture = temporal b.c. of flux term

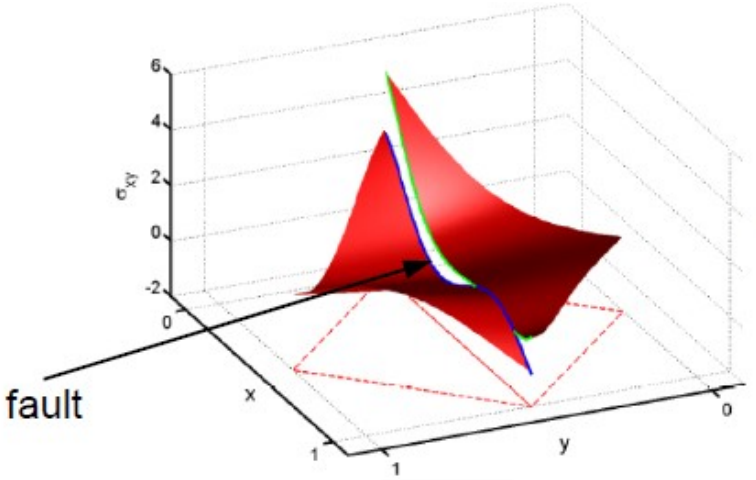

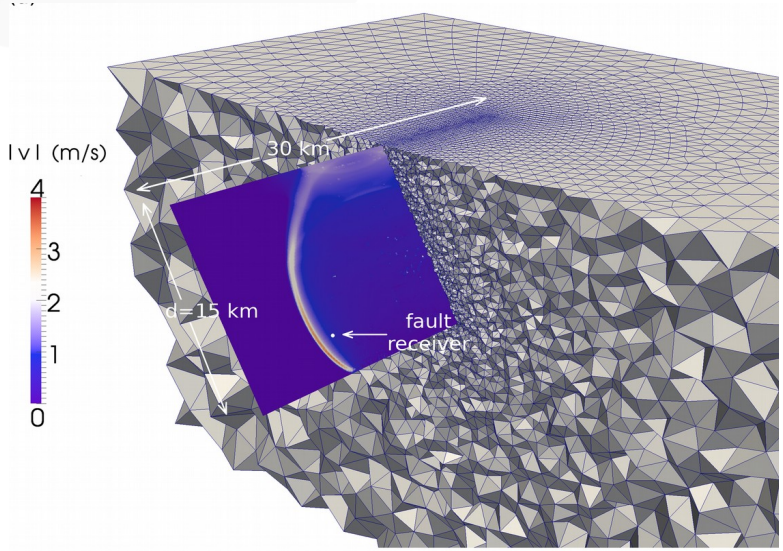

Asymmetric, unstructured mesh discretizing a dipping fault (SCEC benchmark TPV10)

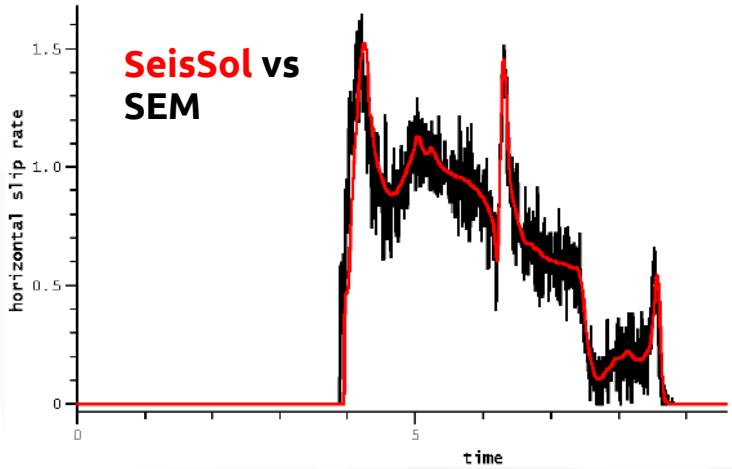

Due to the properties of the exact Riemann solver, the solutions on the fault remain free of spurious oscillations even under complex geometric and physical conditions.

(Pelties, Gabriel and Ampuero, GMD'14)

SeisSol for Dynamic Rupture Simulations

- **tpv16/17:** heterogeneous initial stress

  → resolution of interface wavefront originating at free surface (healing phase followed by high slip rate front)

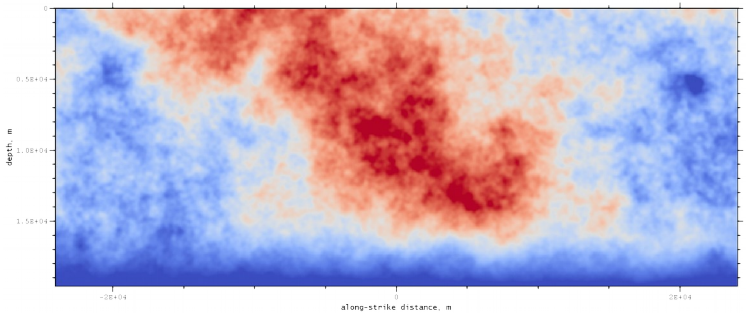

Along-strike slip-rate at on-fault receiver and across the fault at t=5.5 s

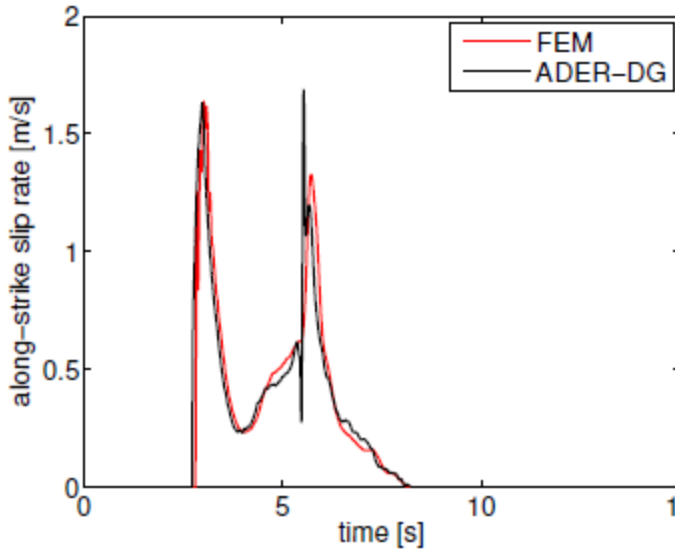

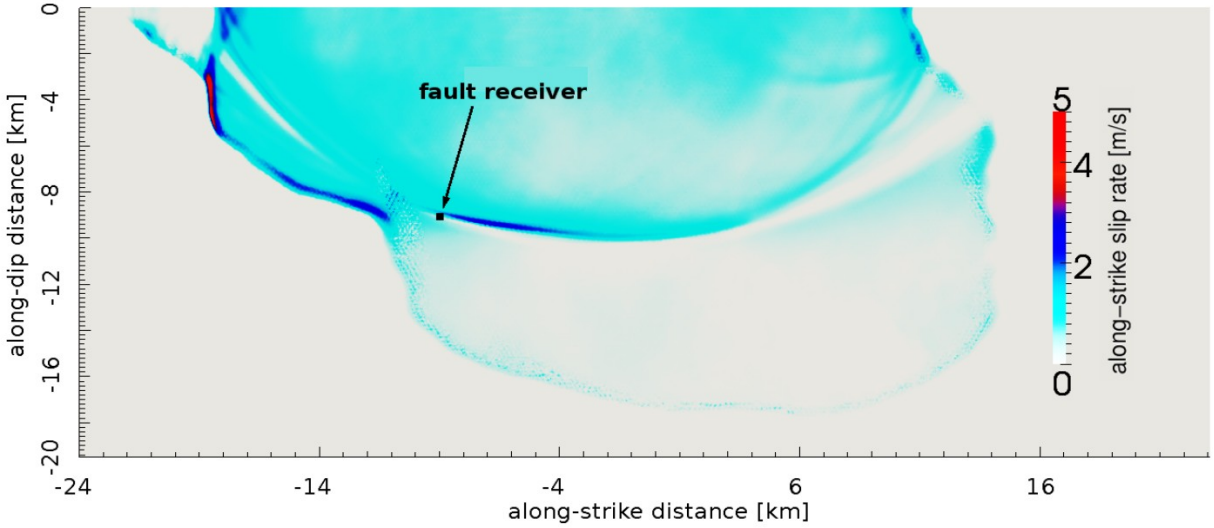

- **tpv13: implementation of off-fault plasticity**

  → element local appliance of yield criterion

  → currently slows down wave propagation core ~ 10%

  → to do: convergence test

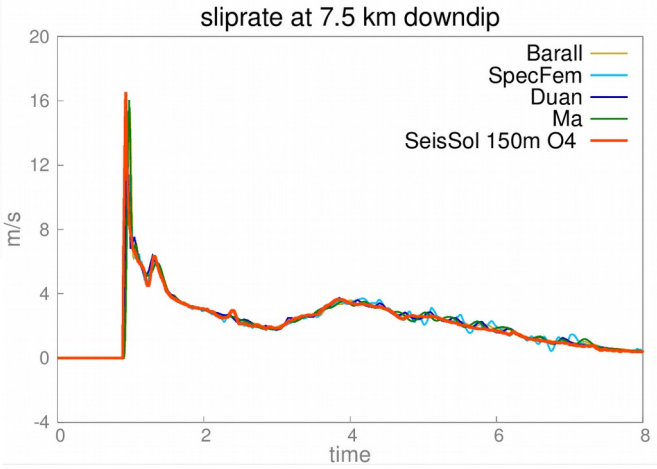

Optimization of SeisSol – Dynamic rupture coupling on heterogeneous architectures

- **Offload Scheme:** hides communication with Xeon Phi and between nodes to address load imbalances of multi-physics simulation

  → Keep accelerators busy at all time, use strong CPU-cores for complex dynamic rupture, overlap communication and computation

- Parallel hybrid MPI+OpenMP parallelization

  → addressing manycore parallelism with 1–3 coprocessors

- Stampede and Tianhe-2: strong scaling @ **90% parallel efficiency and 20% peak performance**
- Tianhe-2: **8.6 PFLOPS** in weak scaling test on 8192 nodes

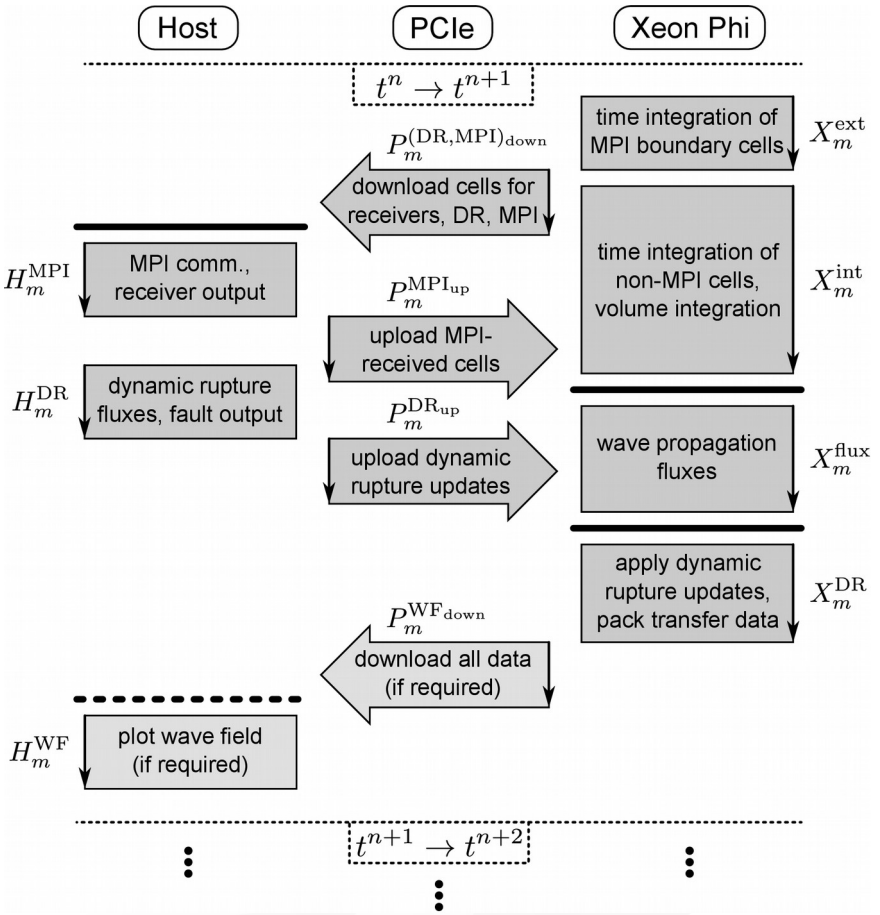

Xeon Phi offload scheme: the multiphysics problem is carefully scheduled to the heterogeneous supercomputer node.

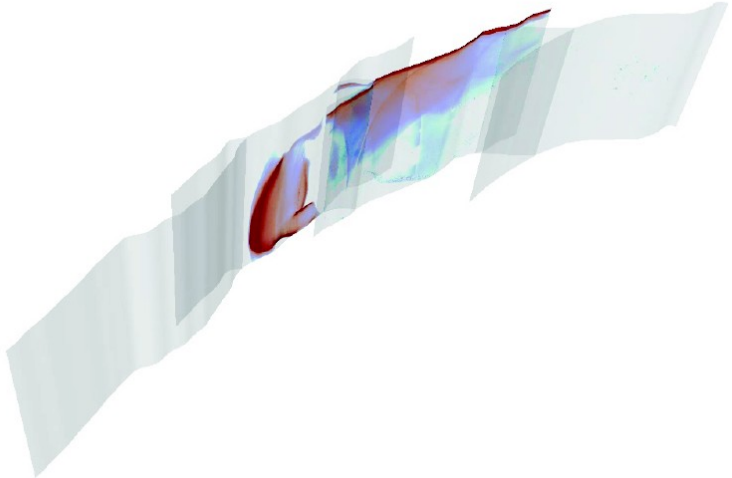

(A. Heinecke et al., Gordon Bell Prize Finalist 2014)

Petascale simulation of a Landers fault system earthquake scenario

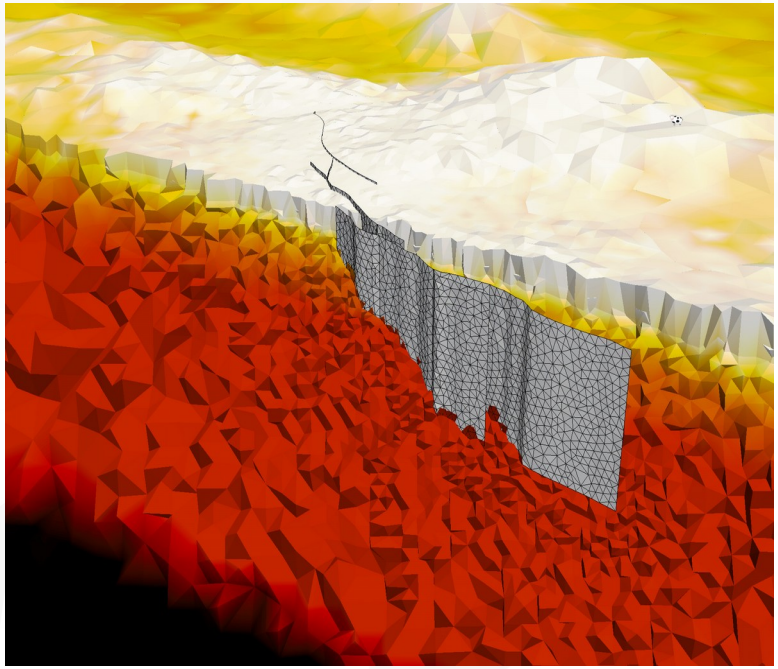

Landers fault system model involving fault geometries, topography, local velocity structure, background stress conditions & fault strength observations.

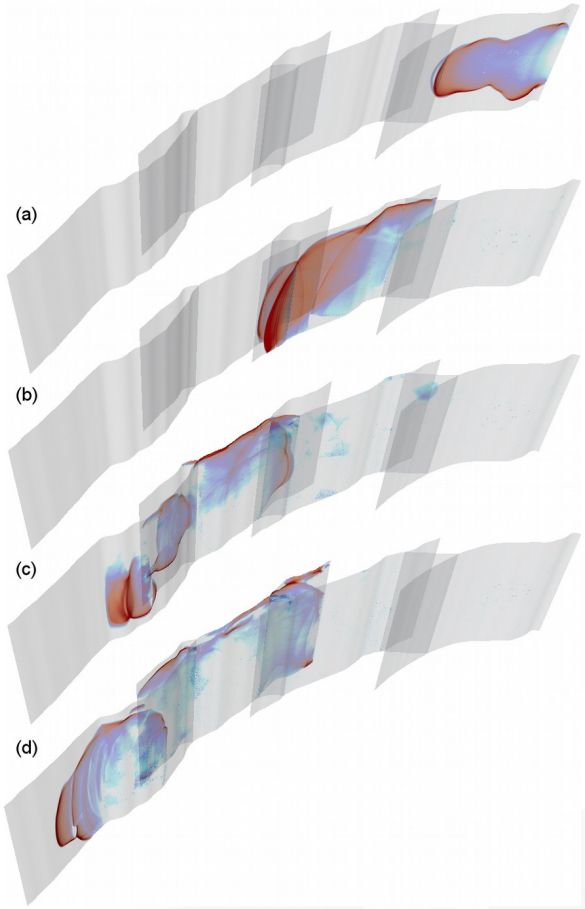

- **Petascale Dynamic Rupture Simulations on Tianhe-2, Stampede and SuperMUC**
- Dynamic earthquake simulation based on the Mw 7.3 1992 Landers event featuring high-detail rupture evolution

Petascale simulation of a Landers fault system earthquake scenario

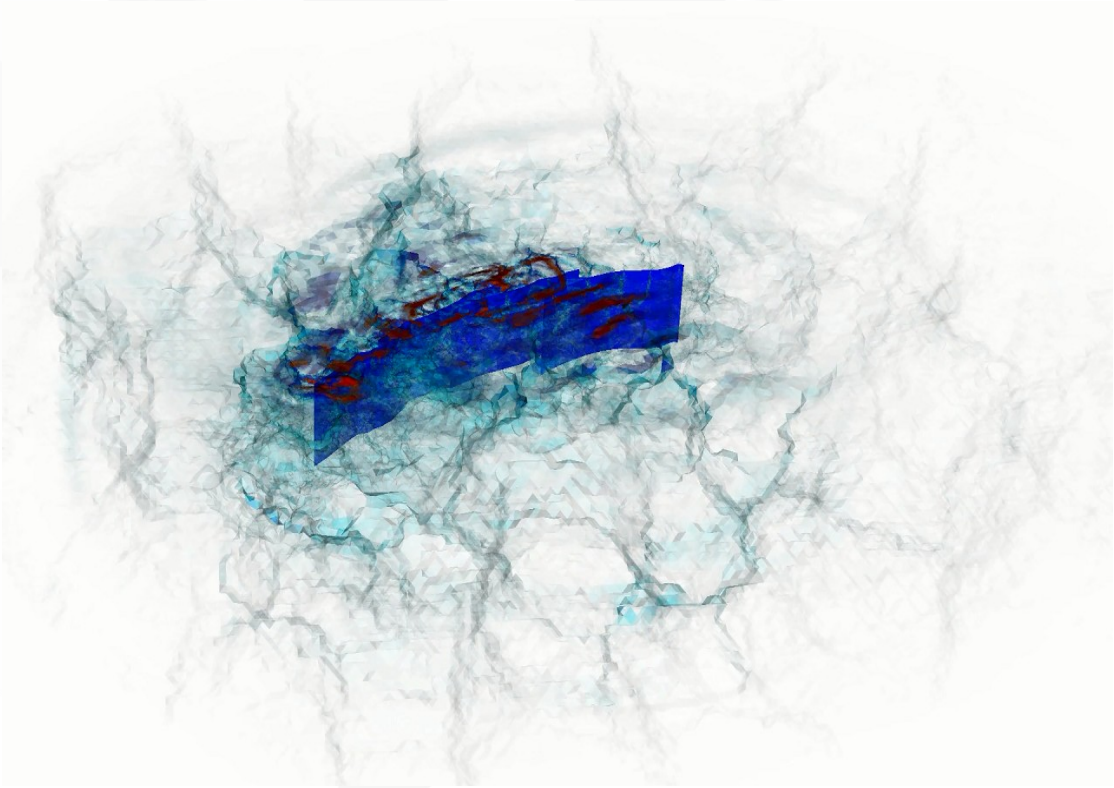

Seismic waves emitted by the complex fault system of the 1992 Landers dynamic rupture earthquake scenario

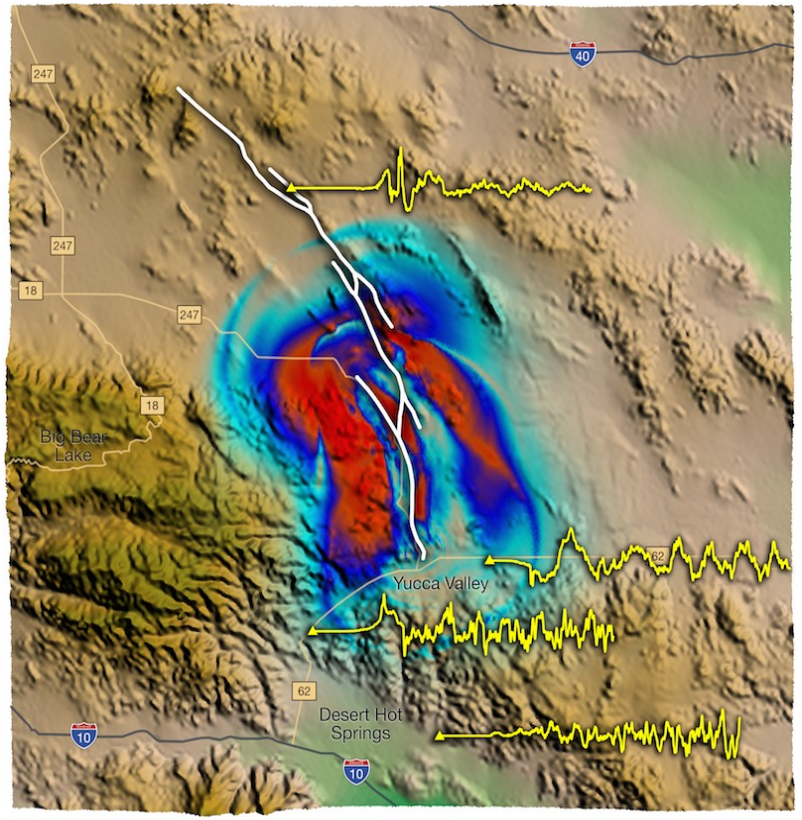

Ground motion of the Landers scenario in terms of absolute particle velocity at the surface. Four seismograms in the direct vicinity of the fault system are depicted exemplary

- ... and ground motion frequencies of 0...10 Hz
- 200x10^6 element mesh (5x10^10 DoF) which ran on ~150 000 cores of SuperMuc for 234,567 time steps (42 seconds simulation time)
- Production run (over 7h of computation time) @ **1.25 PFLOPS** sustained performance

Mw 7.3 '92 Landers earthquake scenario

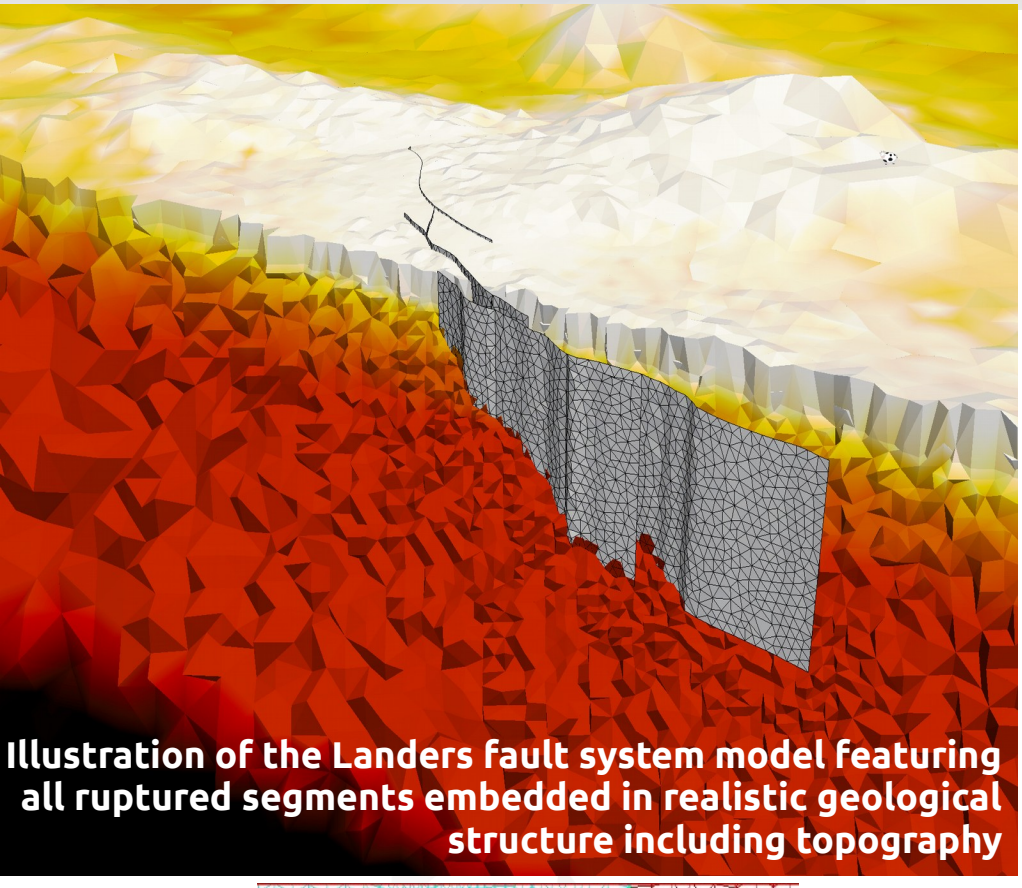

Illustration of the Landers fault system model featuring all ruptured segments embedded in realistic geological structure including topography

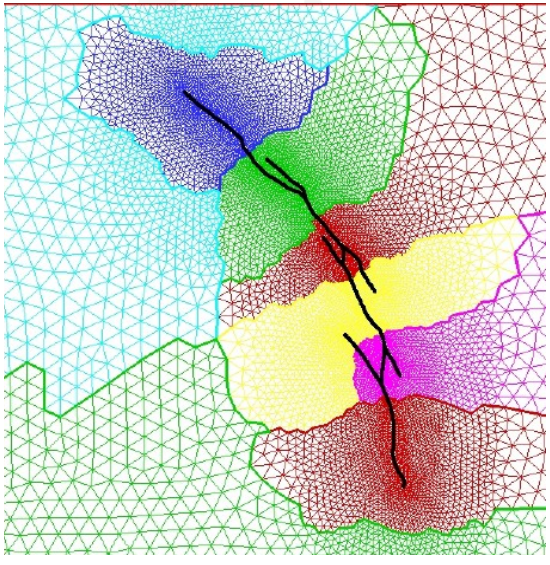

- Earthquake simulation based on the Mw 7.3 1992 Landers event, in which we observed high-detail dynamic rupture evolution and ground motion frequencies of 0...10 Hz relevant for civil engineering purposes

- 85 km **overlapping fault zones**, 5 principal faults of which only 2 slipped totally, large vertical slips, large surface strike-slip offsets, high stress-drop → rare simultaneous failure of several discrete large faults

- **Tectonic setting** and **non-planar** fault structure play significant role in nucleation and rupture process (Olsen et al., 1991, Peyrat et al. 2001, Aochi and Fukuyama, 2002)

- **3D model constructed from observational constraints:**

→ fault geometries (photometry), topography (SRTM), aftershock distributions, local velocity structure (Graves et al.,1998)

Mw 7.3 '92 Landers earthquake scenario

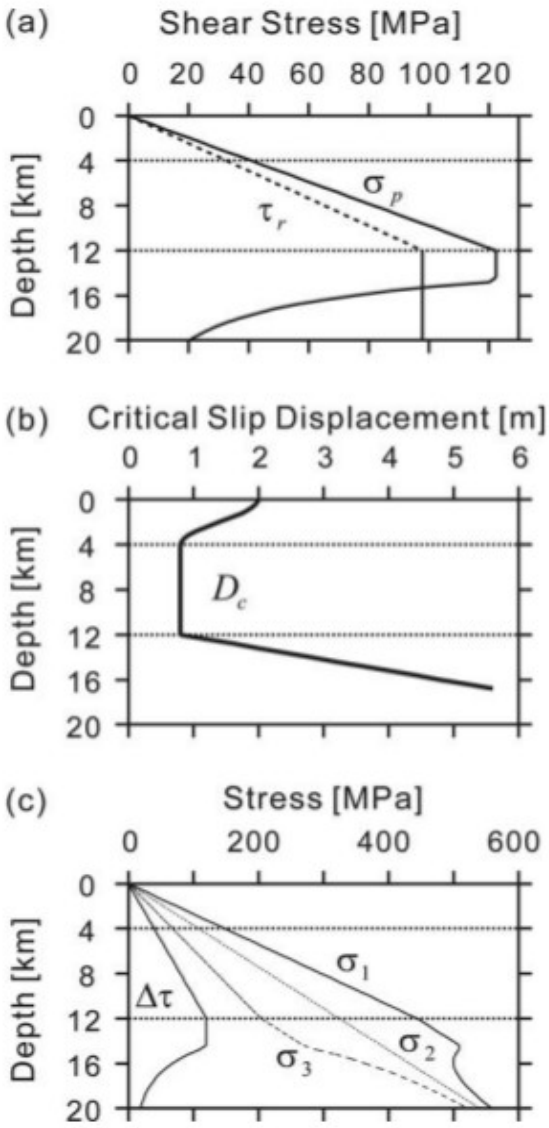

Figure 5. Depth dependence of constitutive parameters and external stress considered in this study: (a) Peak strength σ_p and residual stress level τ_r, (b) critical slip displacement D_c, and (c) magnitudes of principal stress as σ_1, σ_2, and σ_3 and induced maximum shear stress $\Delta\tau = (\sigma_1 - \sigma_3)/2$.

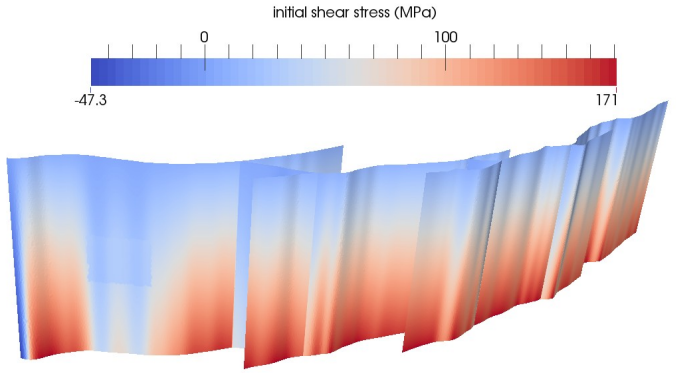

Heterogeneous shear stress distribution along the fault system depending on the fault strike and the direction of the maximum principal stress axis

- **3D model constructed from observational constraints:**

  → **fault strength** from rock mechanics, laboratory experiments and field observations (Aochi and Fukuyama, 2002)

Mw 7.3 '92 Landers earthquake scenario

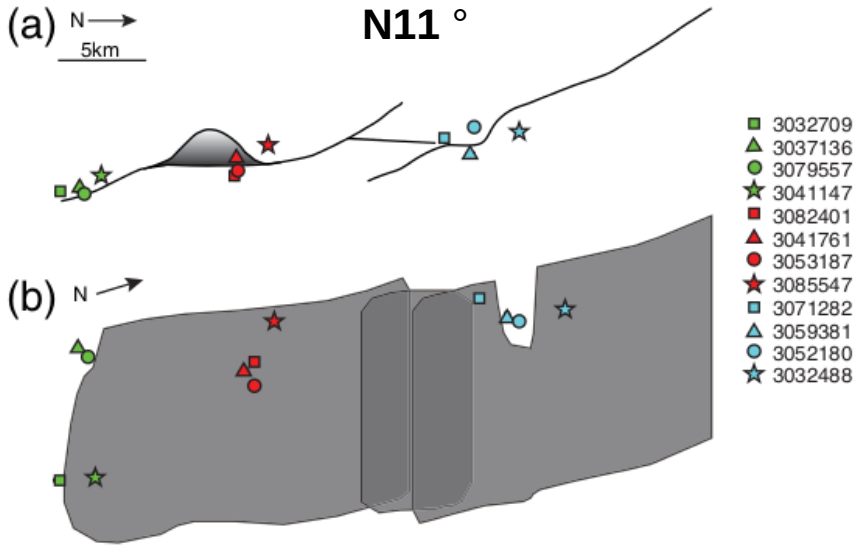

Figure 11. Preferred model geometry, (a) in map-view and (b) in an oblique view, looking northwest. Icons show the locations of analyzed aftershocks. The JVF extends farther south below the surface than all original models, passing northeast of the location of event 3032709, and dips 75° W along its central extent. The HVF is discontinuous for 3 km along fault strike and to 3 km depth through the slip gap.

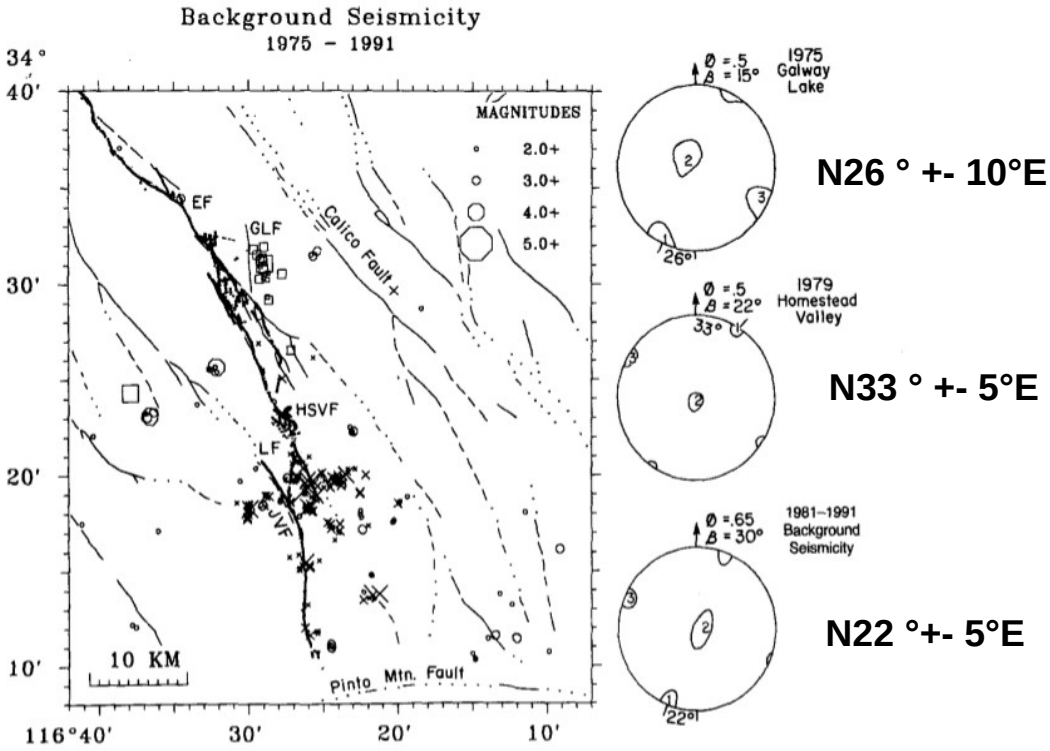

Figure 4. Results from the stress inversion of focal mechanisms from the following: (1) Galway Lake 1975, shown with square symbols; (2) Homestead Valley 1979, shown with x symbols; and (3) background seismicity near Landers 1981 to 1991, shown with circles (see also Fig. 2 for labeling of stresses).

→ **background stress conditions** (direction of max. compressive stress) from geomechanical modeling (Madden and Pollard, 2012) or stress inversion (Hauksson et al., 1995)

Mw 7.3 '92 Landers earthquake scenario

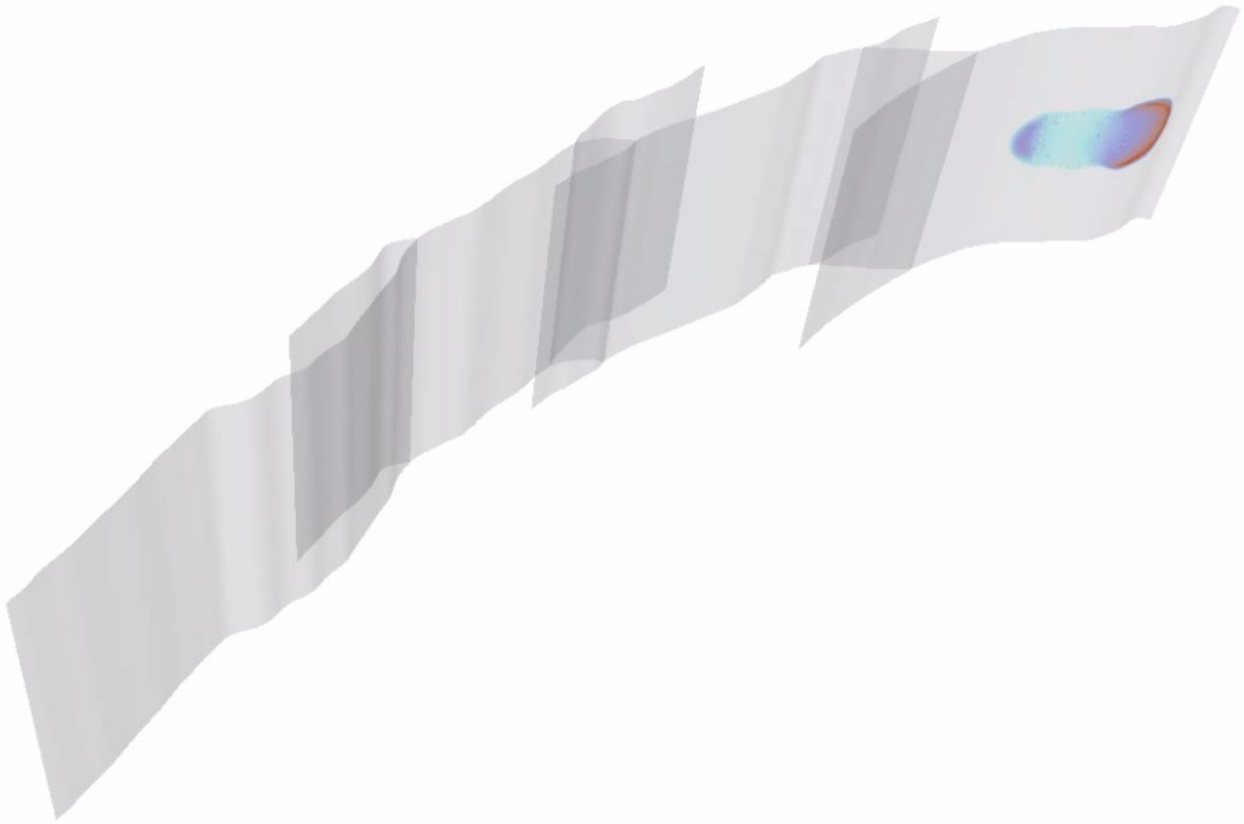

Mw 7.3 '92 Landers earthquake scenario

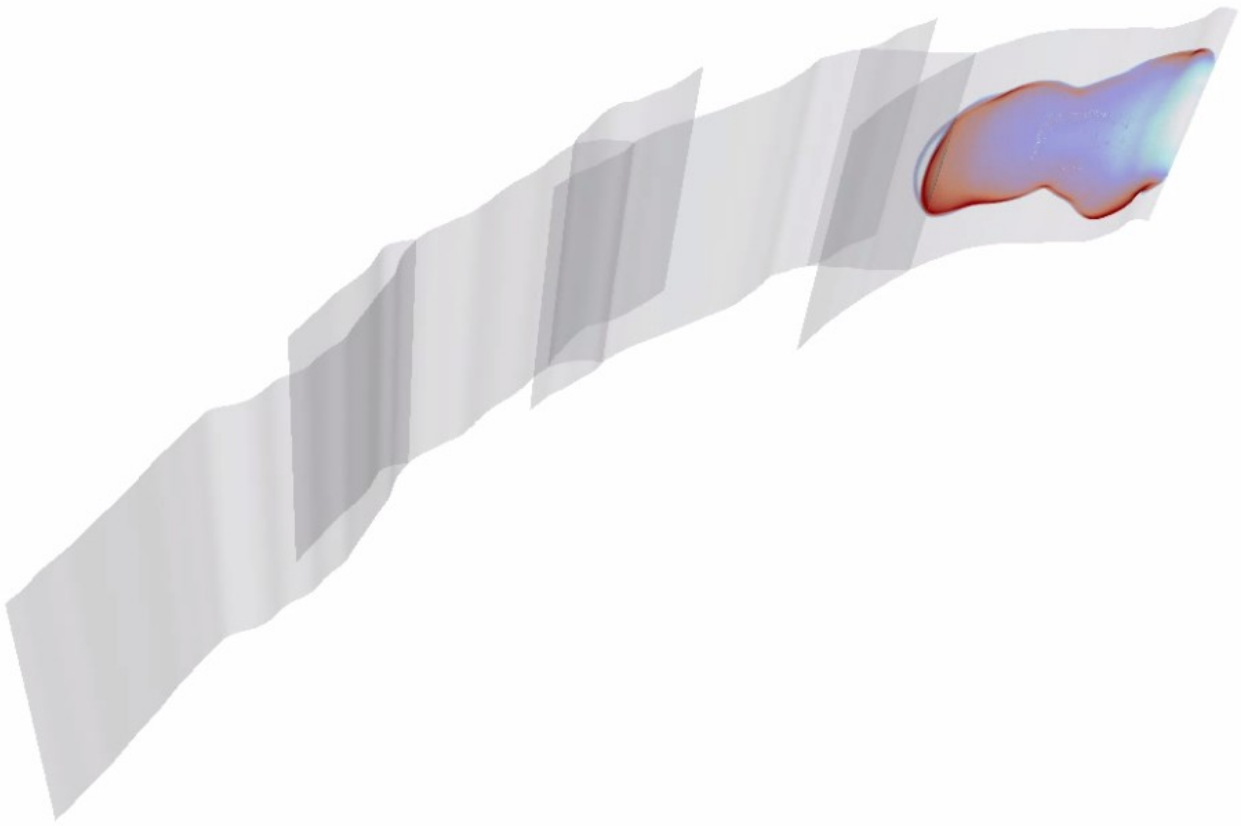

Mw 7.3 '92 Landers earthquake scenario

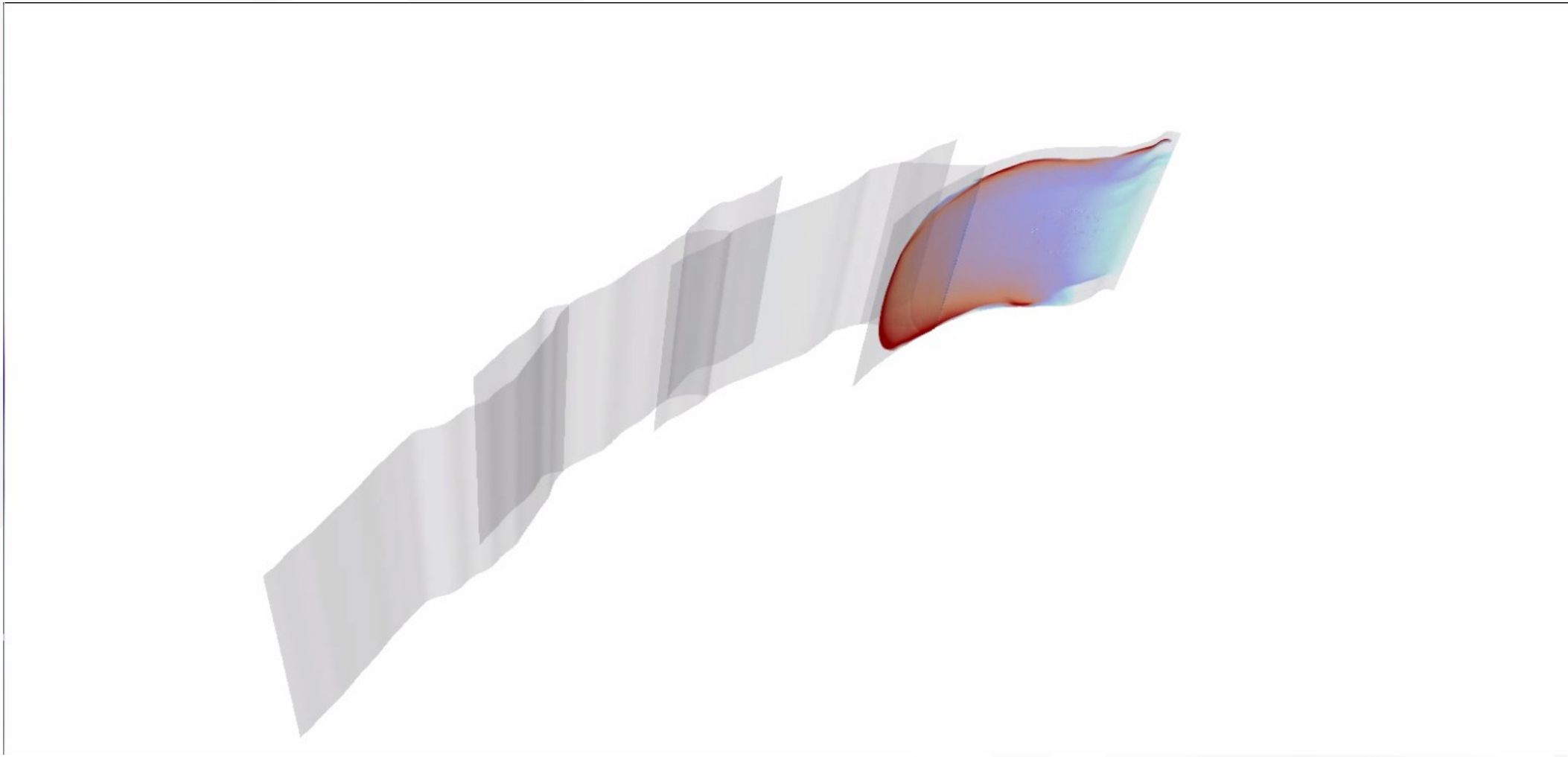

Mw 7.3 '92 Landers earthquake scenario

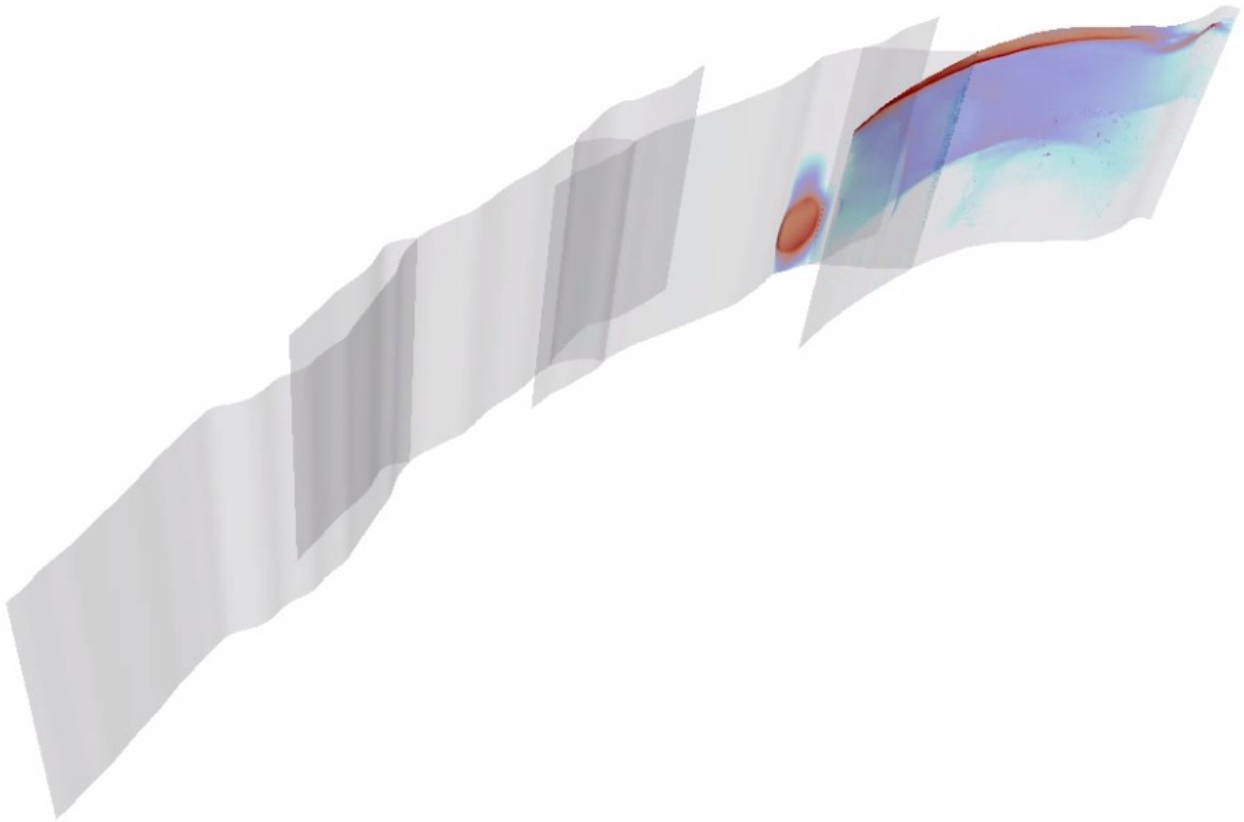

Mw 7.3 '92 Landers earthquake scenario

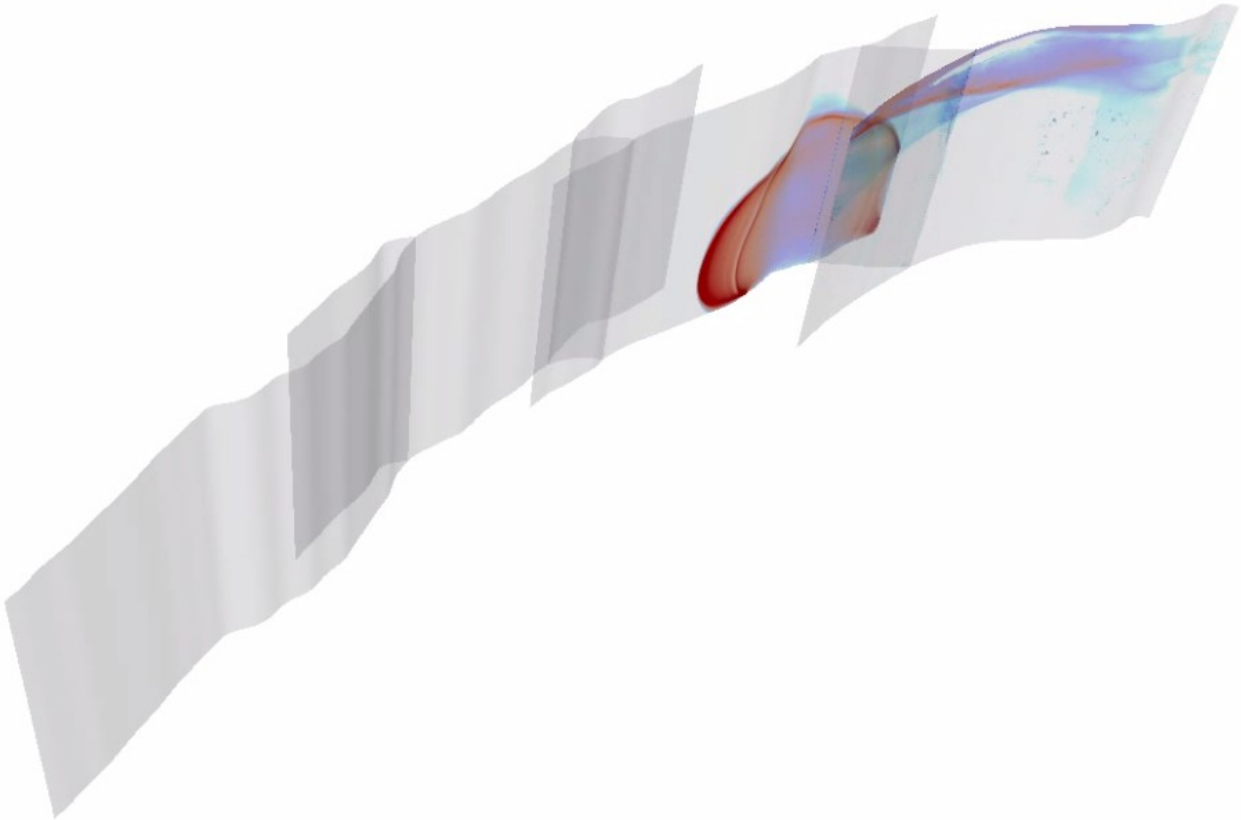

Mw 7.3 '92 Landers earthquake scenario

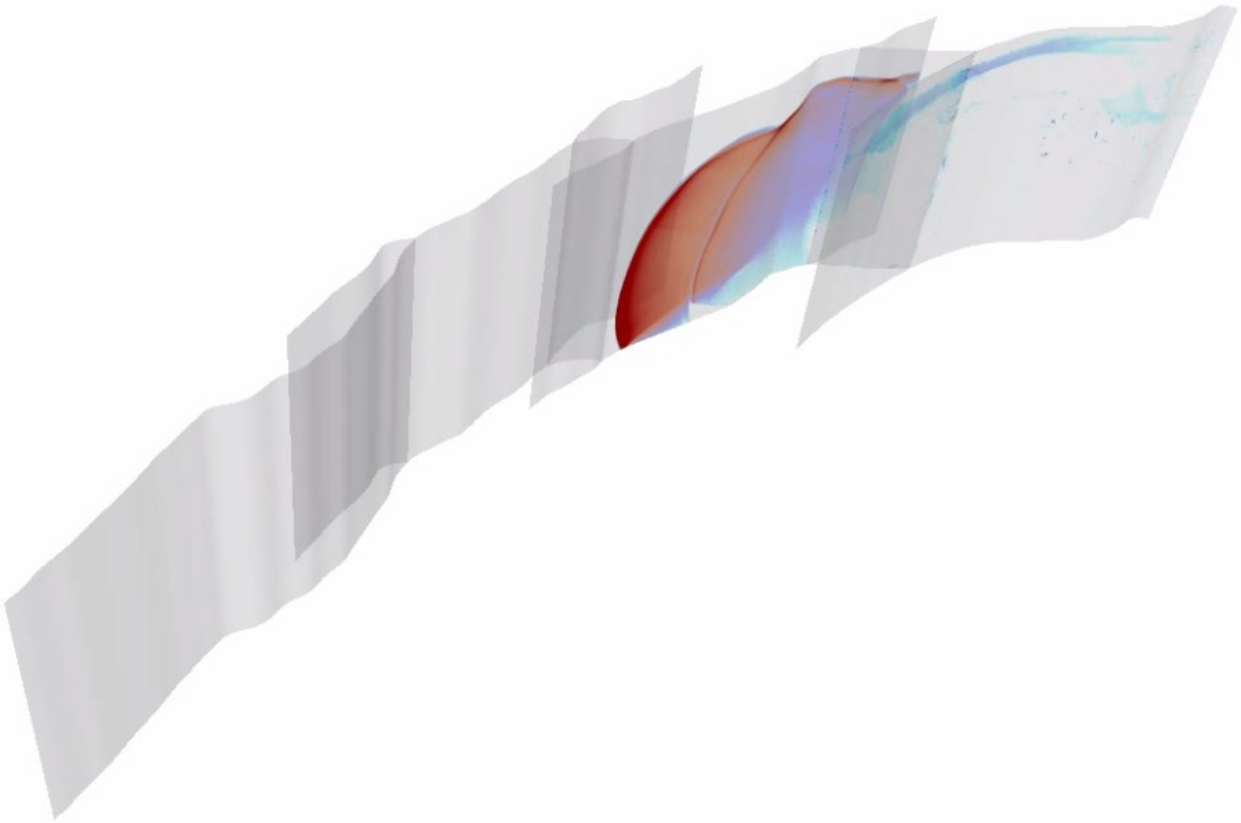

Mw 7.3 '92 Landers earthquake scenario

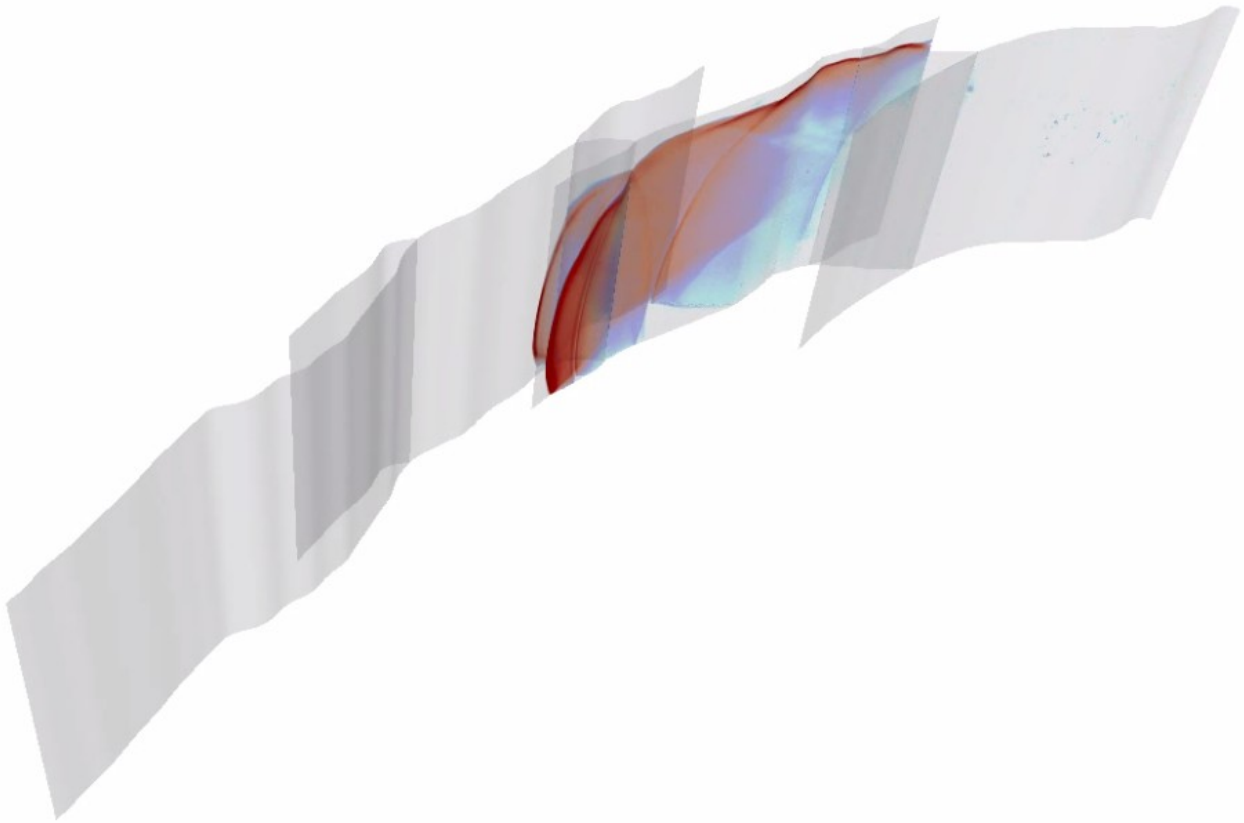

Mw 7.3 '92 Landers earthquake scenario

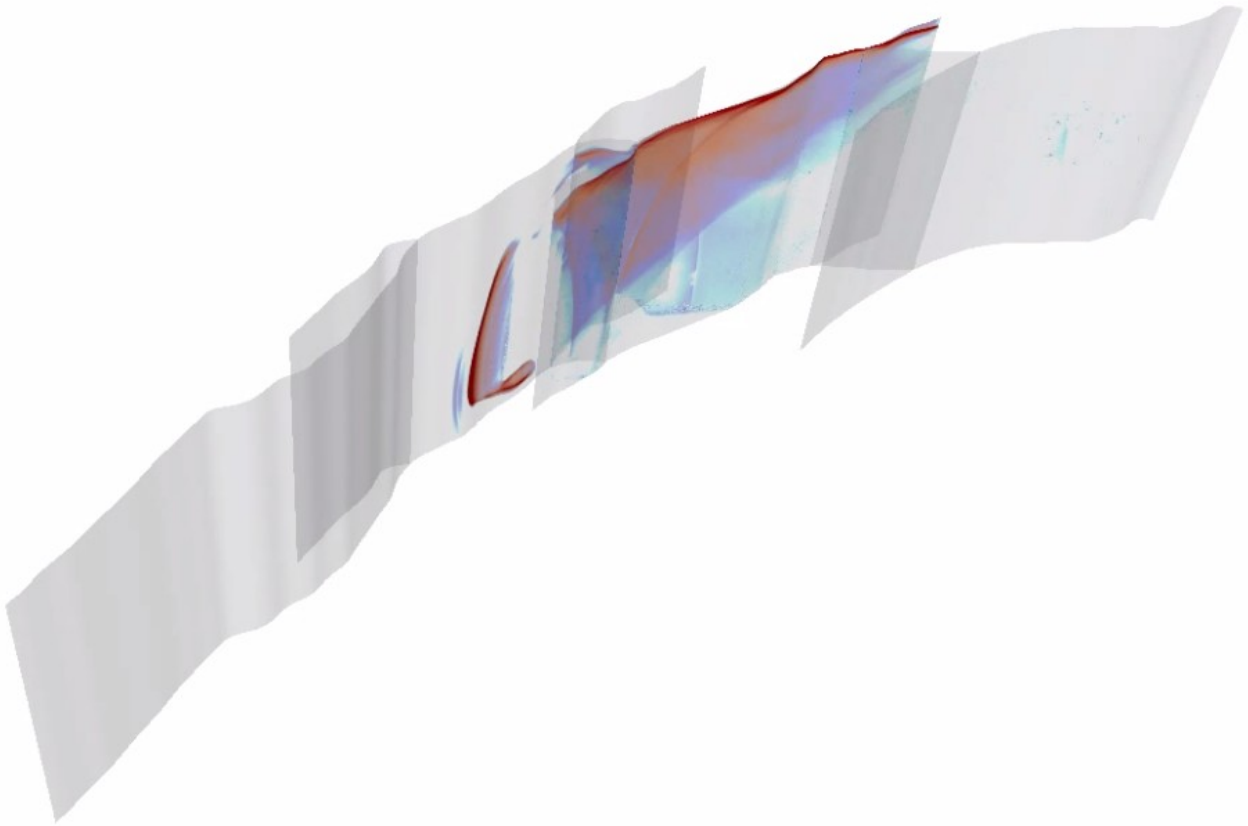

Mw 7.3 '92 Landers earthquake scenario

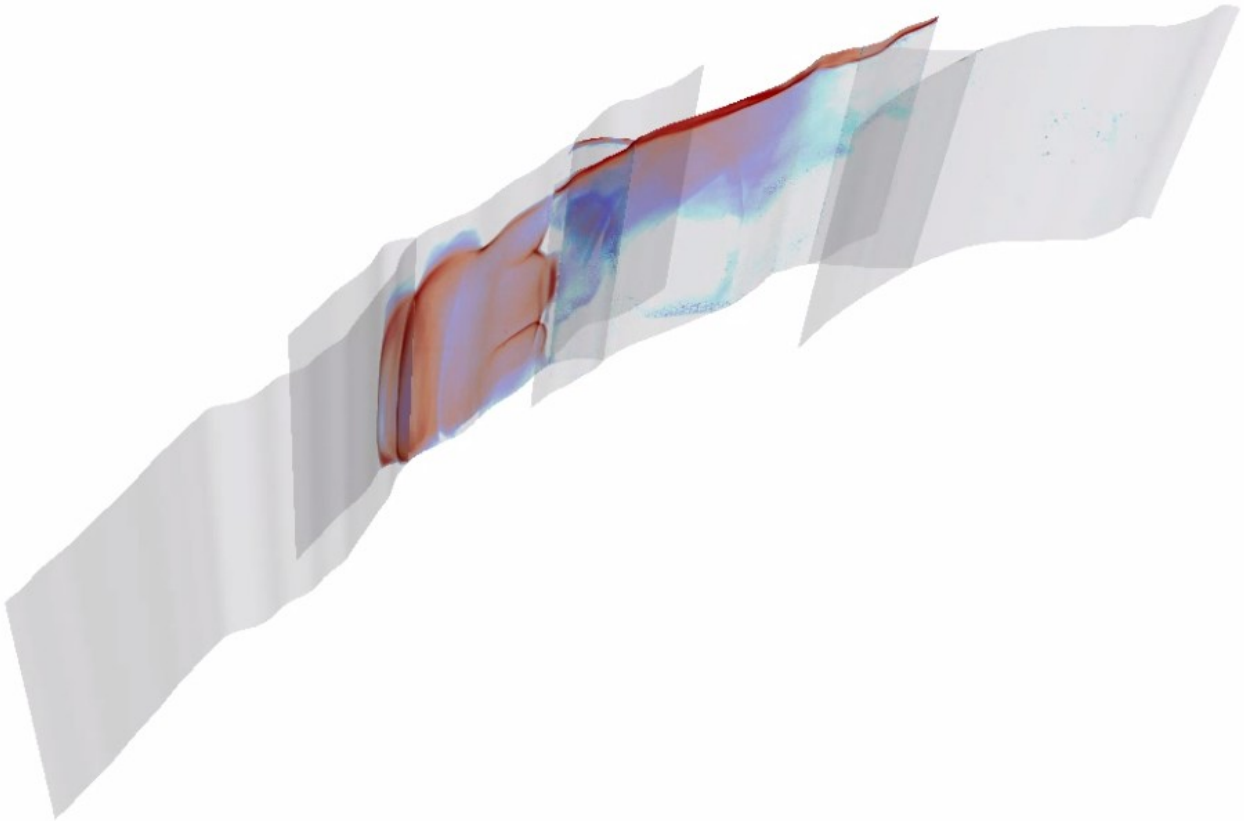

Mw 7.3 '92 Landers earthquake scenario

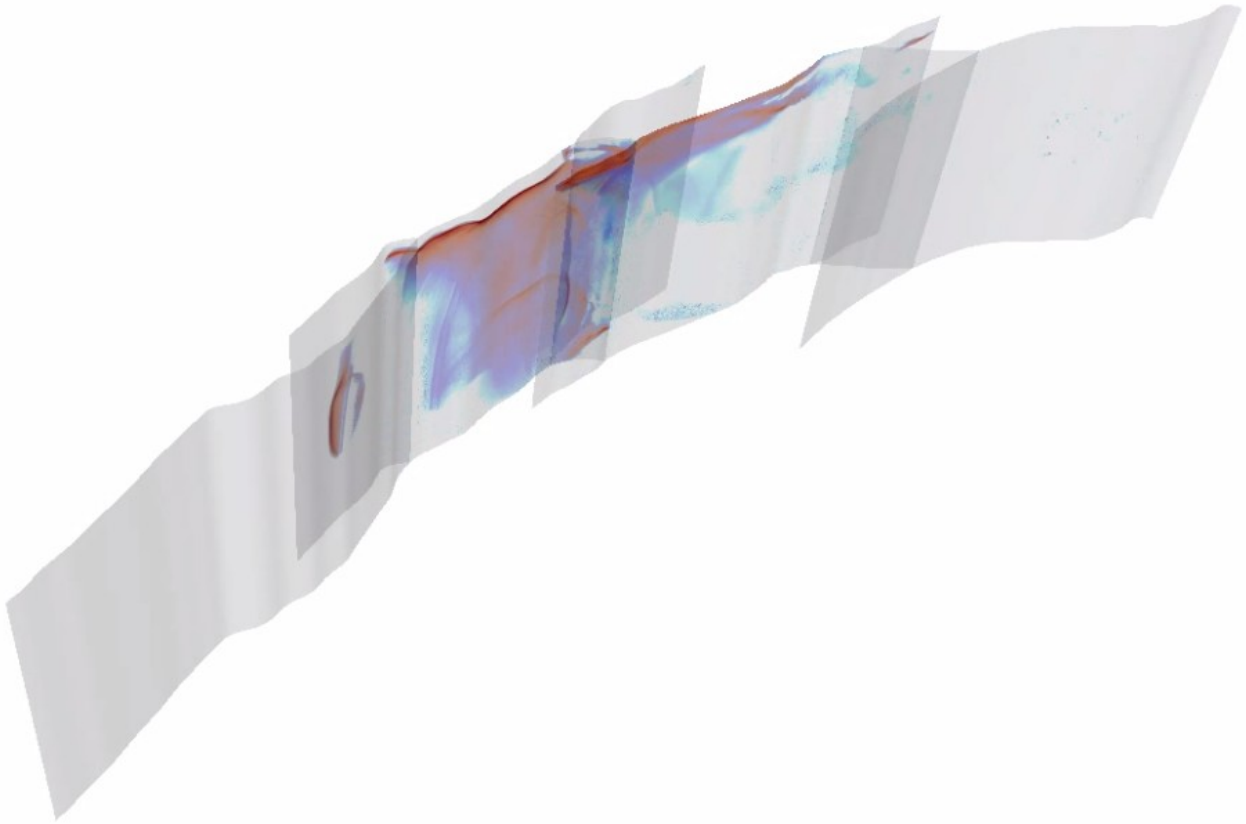

Mw 7.3 '92 Landers earthquake scenario

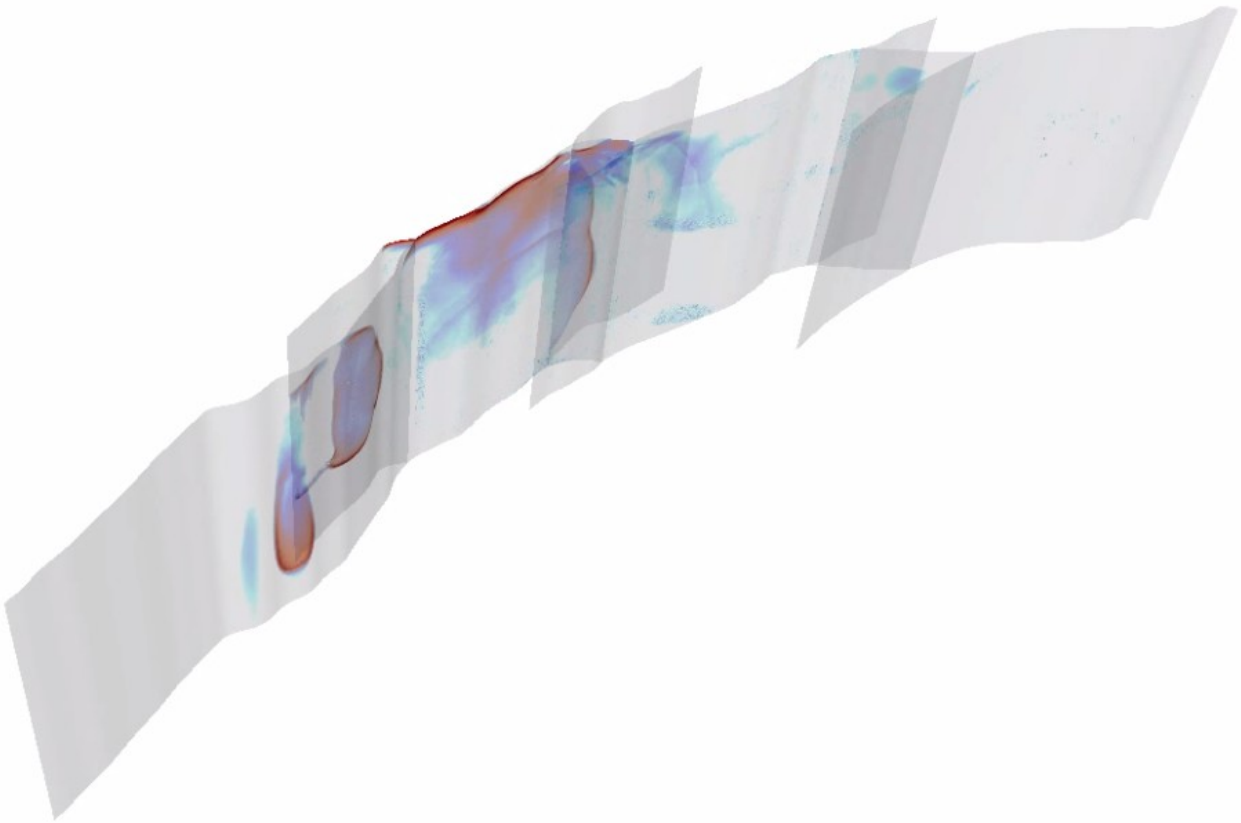

Mw 7.3 '92 Landers earthquake scenario

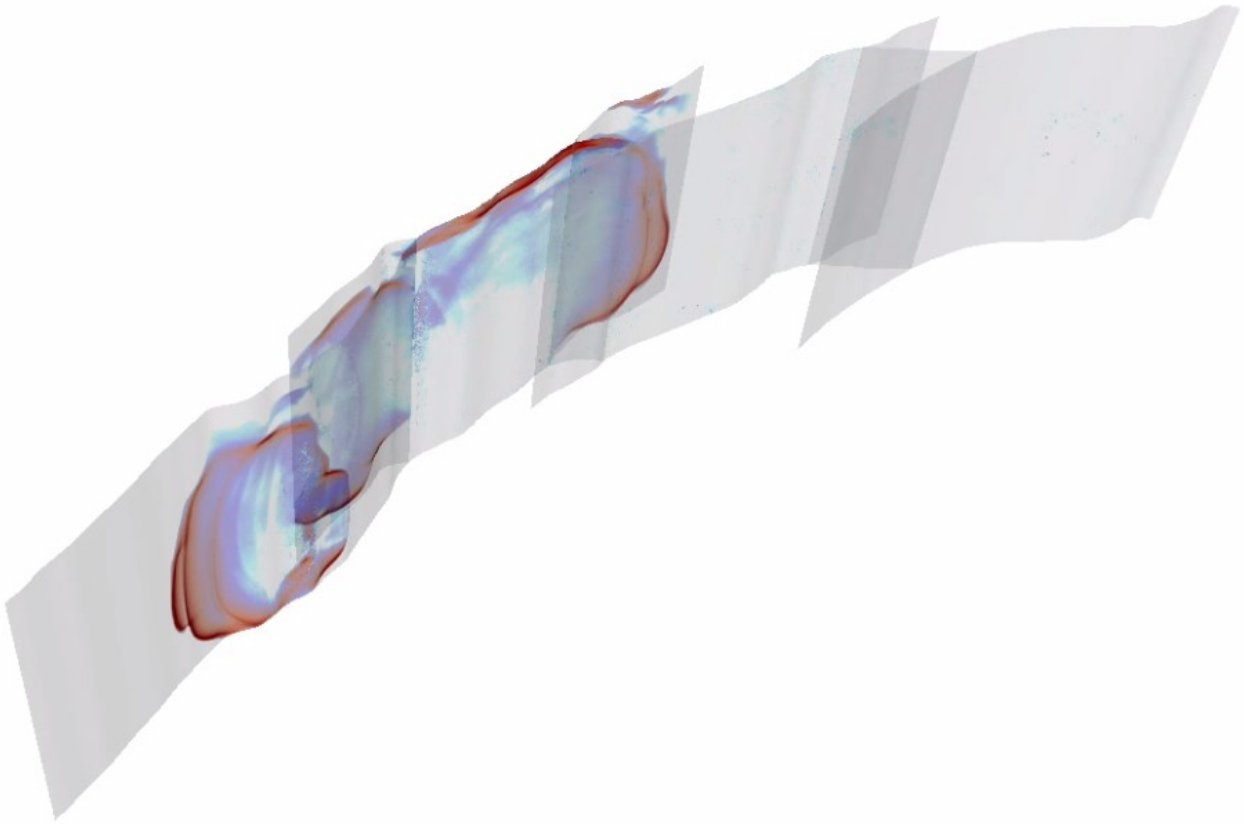

Mw 7.3 '92 Landers earthquake scenario

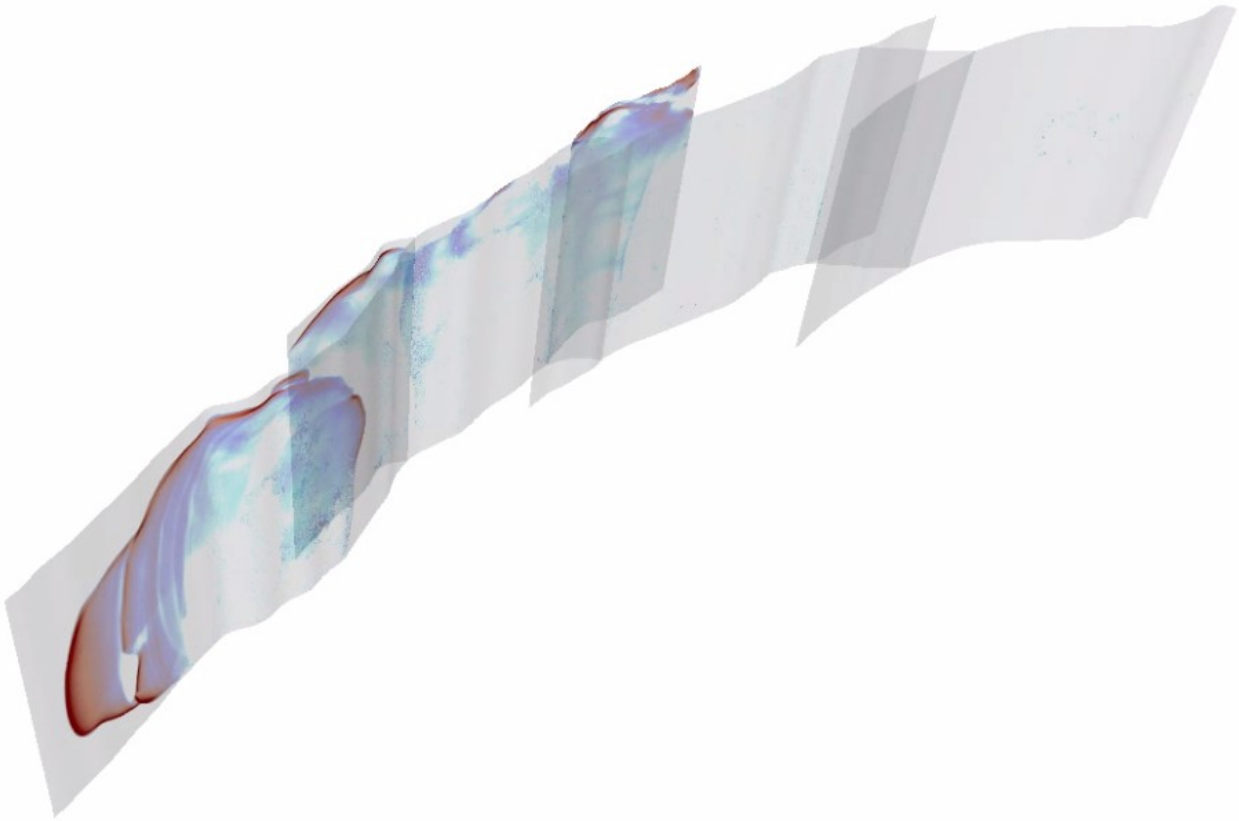

Mw 7.3 '92 Landers earthquake scenario

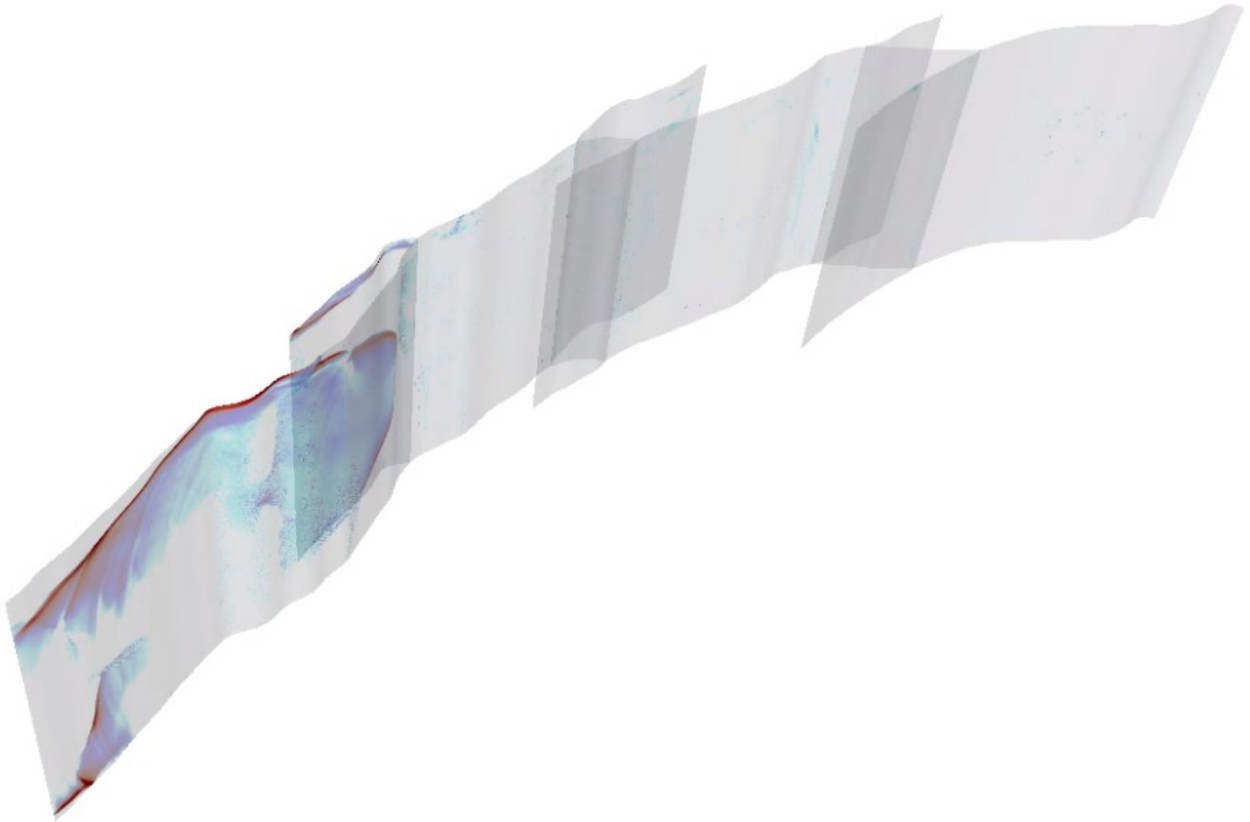

Mw 7.3 '92 Landers earthquake scenario

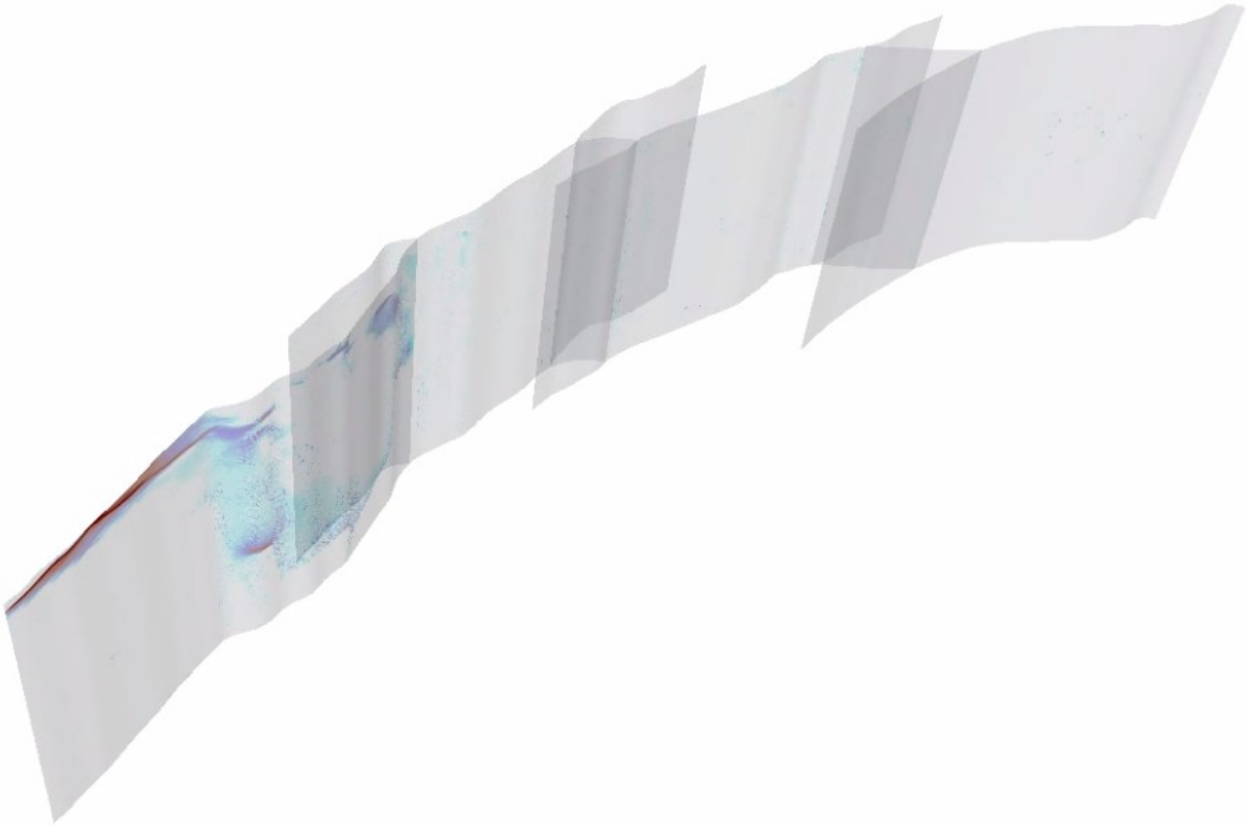

Mw 7.3 '92 Landers earthquake scenario

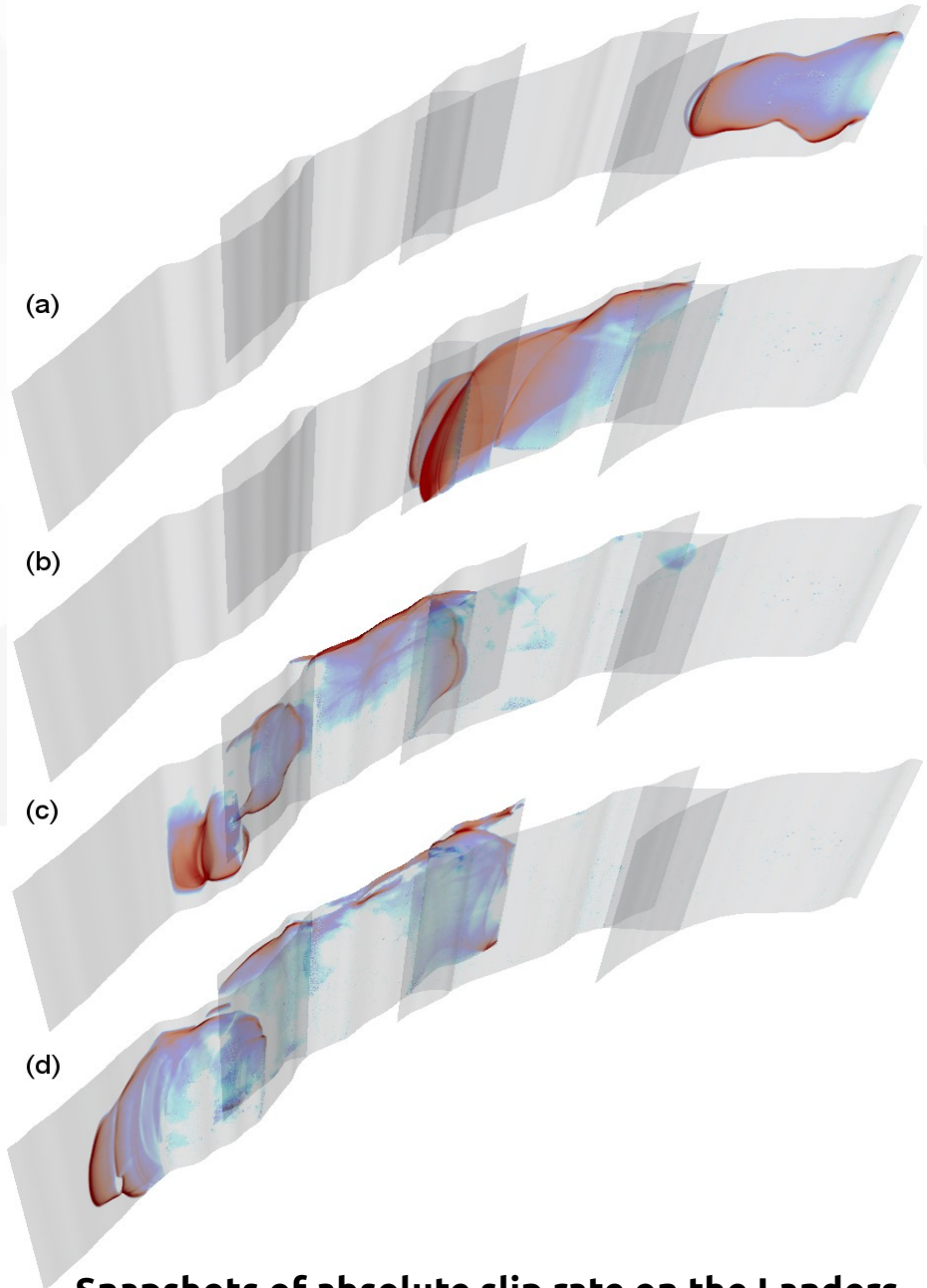

Snapshots of absolute slip rate on the Landers fault system throughout the dynamic earthquake rupture process.

- Dynamic rupture transfers between principal faults in terms of **jumps** and **branching**

→ **reverse slip** in the vicinity of fault branches

- Non-linear interaction of seismic waves with fault system, free surface and heterogeneous rupture process

→ emergence of **multiple rupture fronts**

- High dependence of earthquake dynamics on orientation and amplitude of the **background stress state** concurrently with **fault geometry** (nucleation, branching, slip gap)

Mw 7.3 '92 Landers earthquake scenario

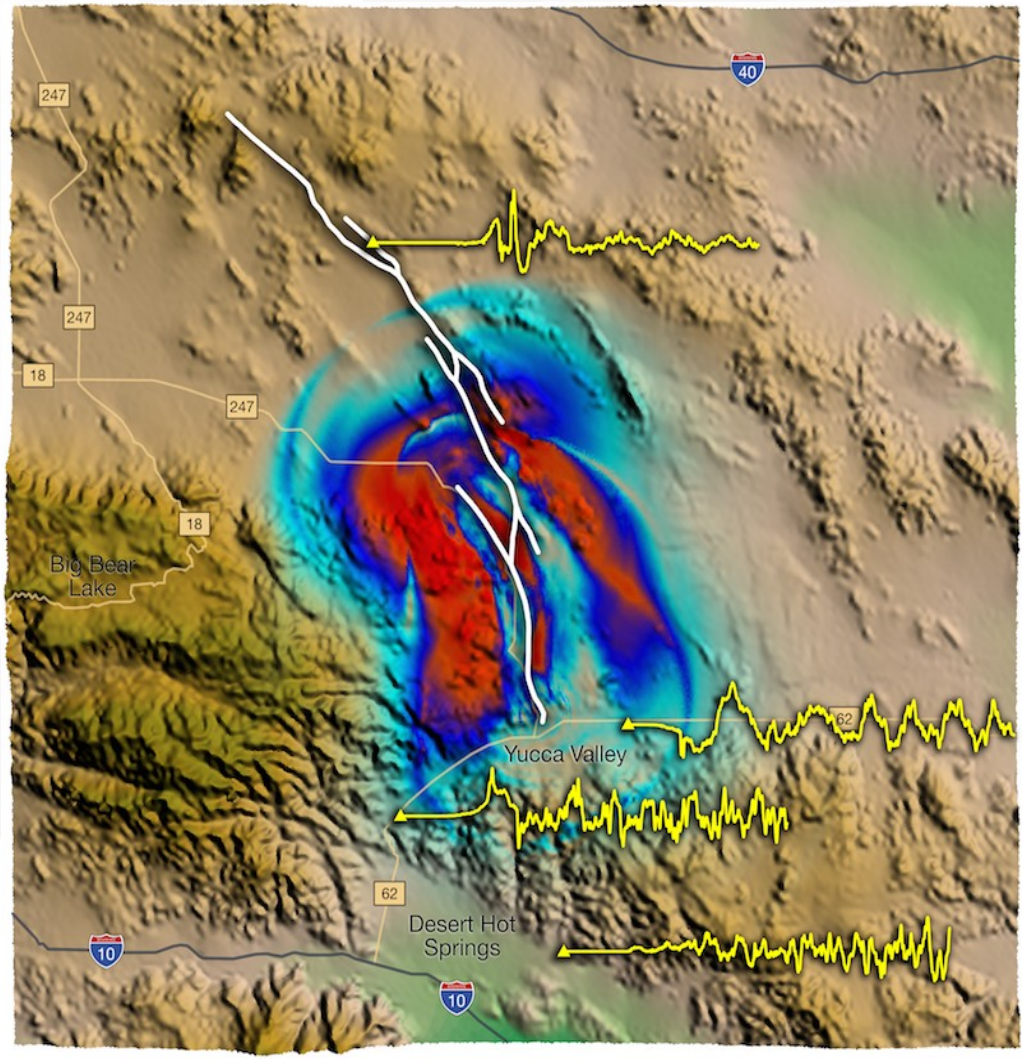

Ground motion of the Landers scenario in terms of absolute particle velocity at the surface. Four seismograms in the direct vicinity of the fault system are depicted exemplary.

- Despite the complexity, the **kinematics** in terms of rupture speed, magnitude, and slip distribution are reasonably well reproduced
- **High-frequent signals** caused by rupture complexity and the interaction of earthquake dynamics and seismic wave propagation with fault complexity and regional topography (no stochastic model ingredients)
- **Large-scale HPC** runs are necessary to resolve ground shaking in the engineering frequency band

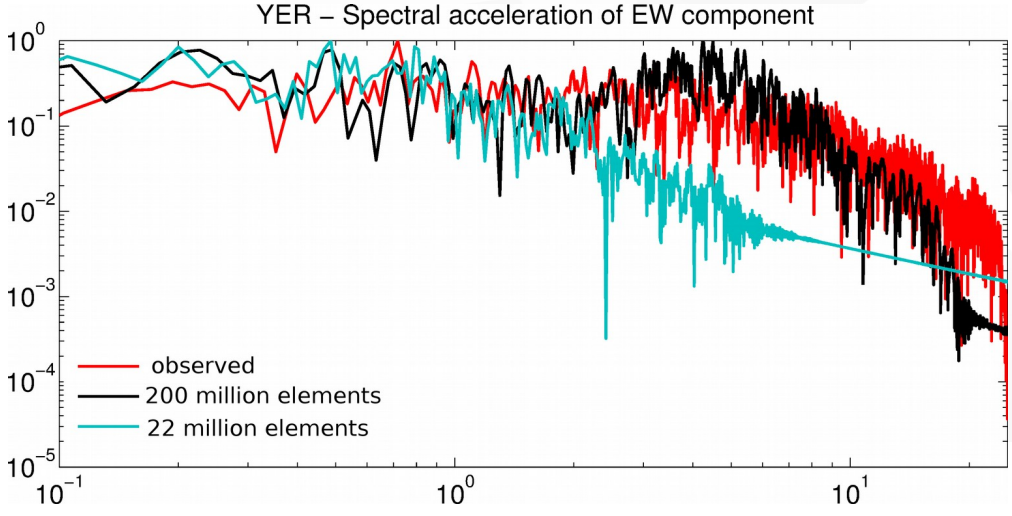

Mw 6.7 Northridge earthquake scenario

- Large scale earthquake scenario based on the Mw 6.7 1994 Northridge blind thrust event including different representations of model complexity

Constraints from observation

- High-resolution topography data
- SCEC Community Fault Model
- SCEC Community Velocity Model

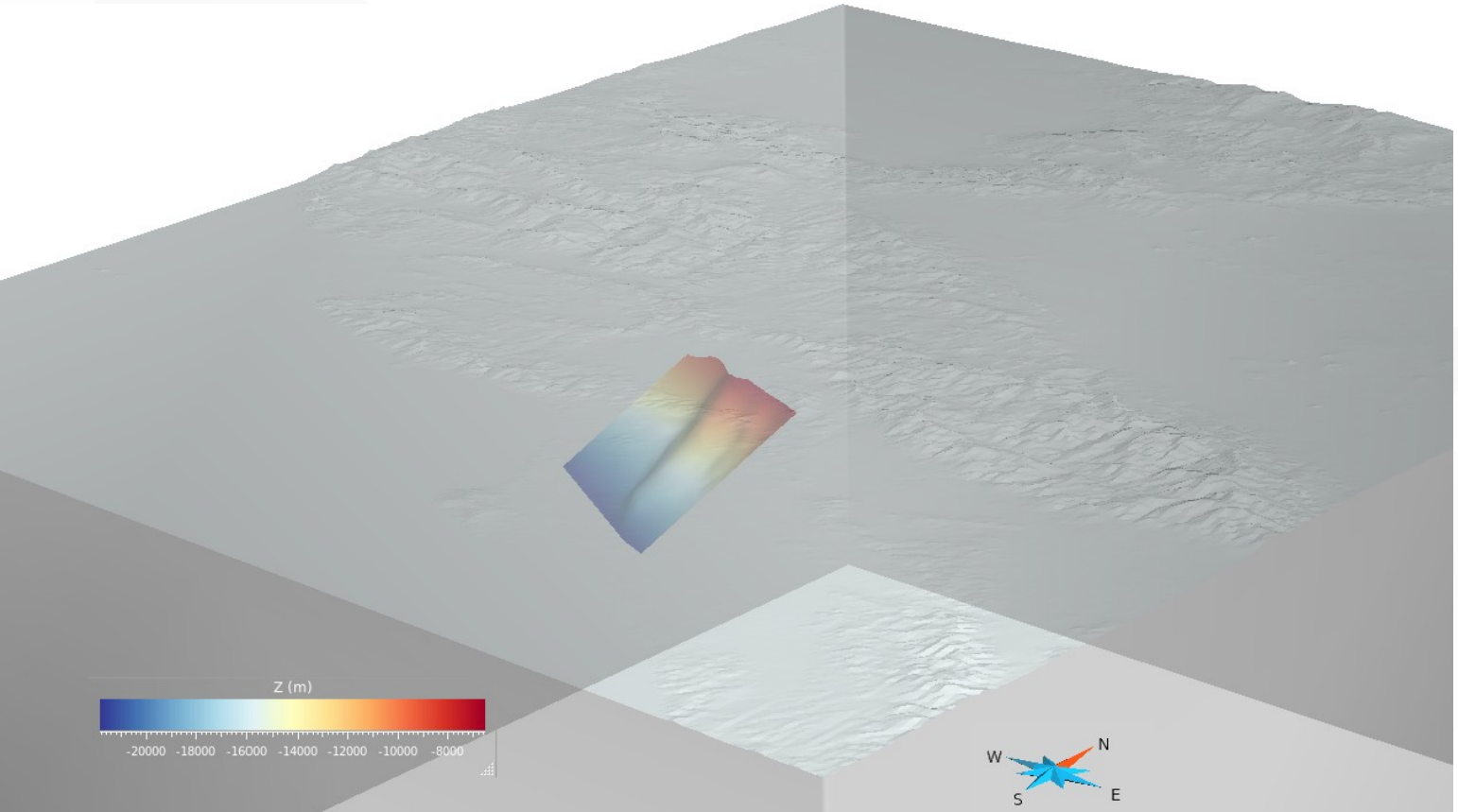

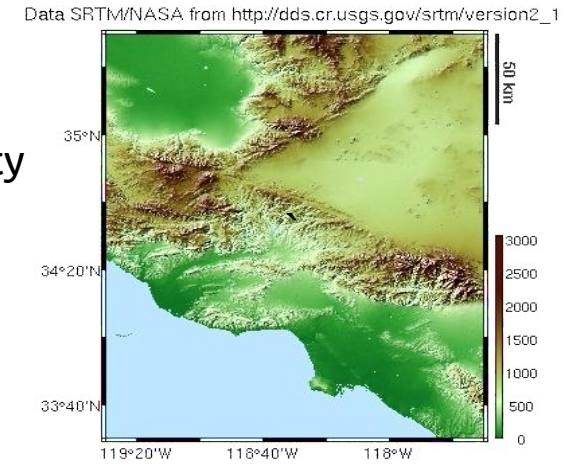

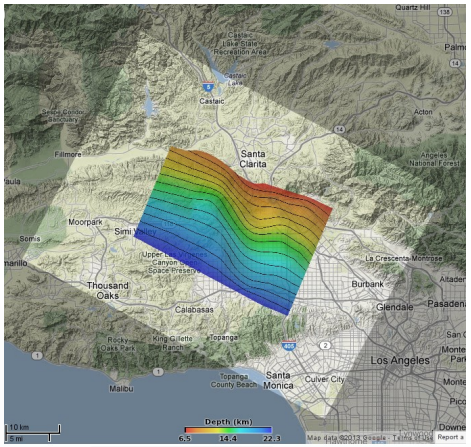

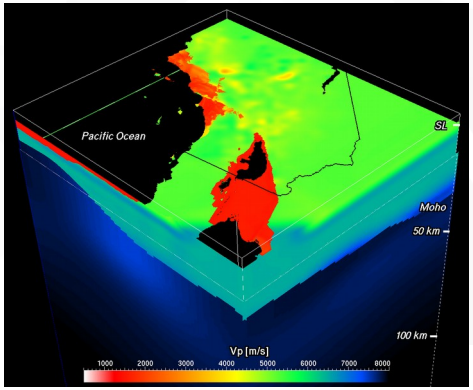

Mw 6.7 Northridge earthquake scenario

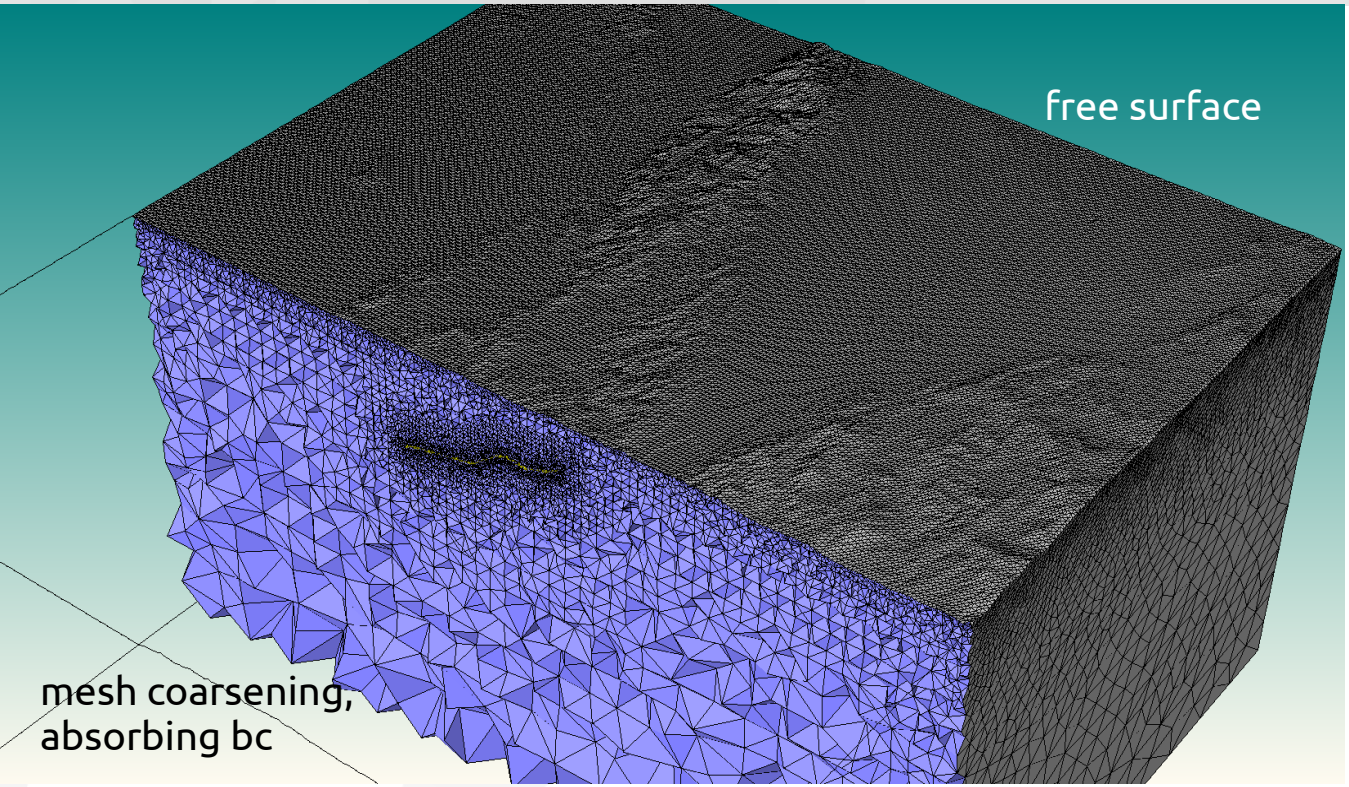

Tetrahedral meshing with SimModeler (Simmetrix): 2.2 million elements, 1 km topography sampling, 500m fault sampling

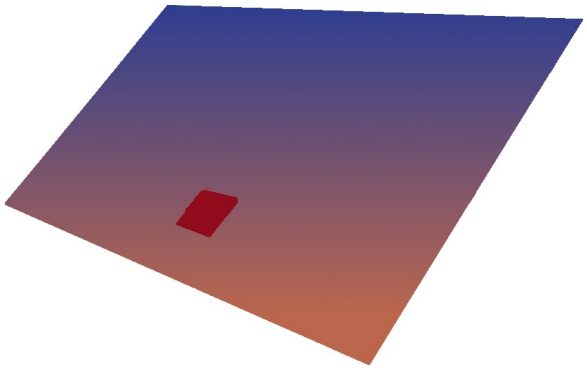

homogeneous depth-dependent background stress

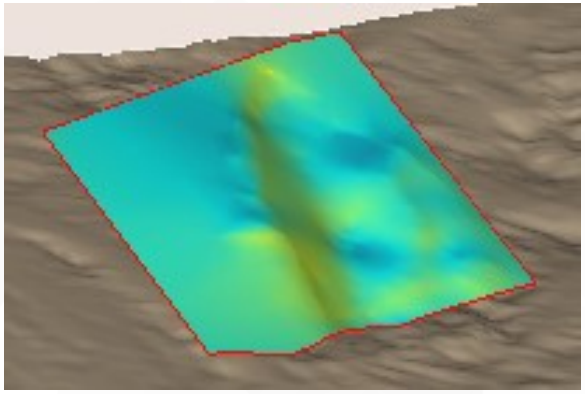

heterogeneous stress state generated by varying dip angle of fault topography

- low resolution: 2.2x10^6 element mesh running on 256 cores for 4 hours (1000 CPUh) simulating 15 s at 1.5 Hz with spatial and temporal order 5

- high resolution: 75x10^6 element mesh running on ~150 000 cores for 3 hours (230 000 time steps) simulating 50 s at ~10 Hz with order 6

Mw 6.7 Northridge earthquake scenario

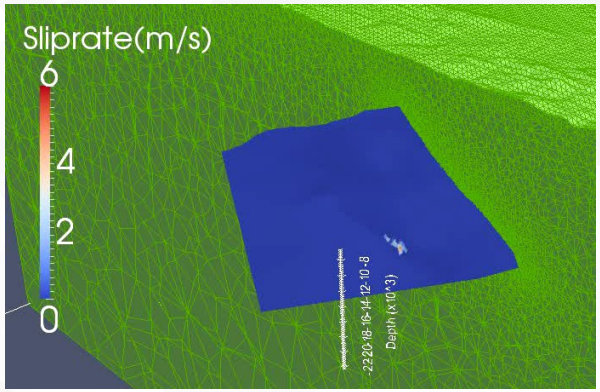

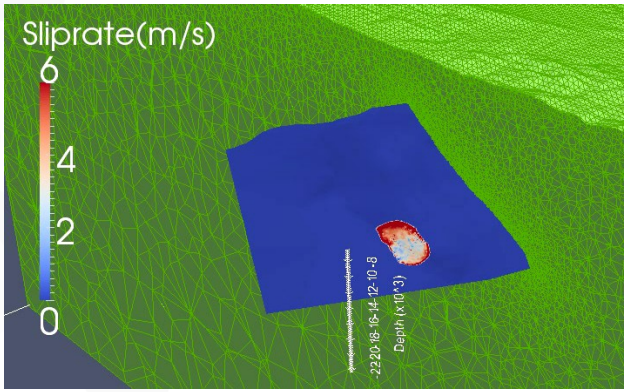

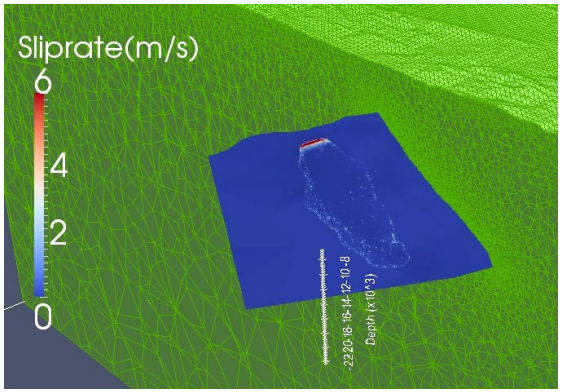

- Dynamic rupture takes a **pulse-like** form independent of resolution and friction parametrization, caused by the effective stress heterogeneity on the curved fault generated by the fault geometry and the regional homogeneous background stress field

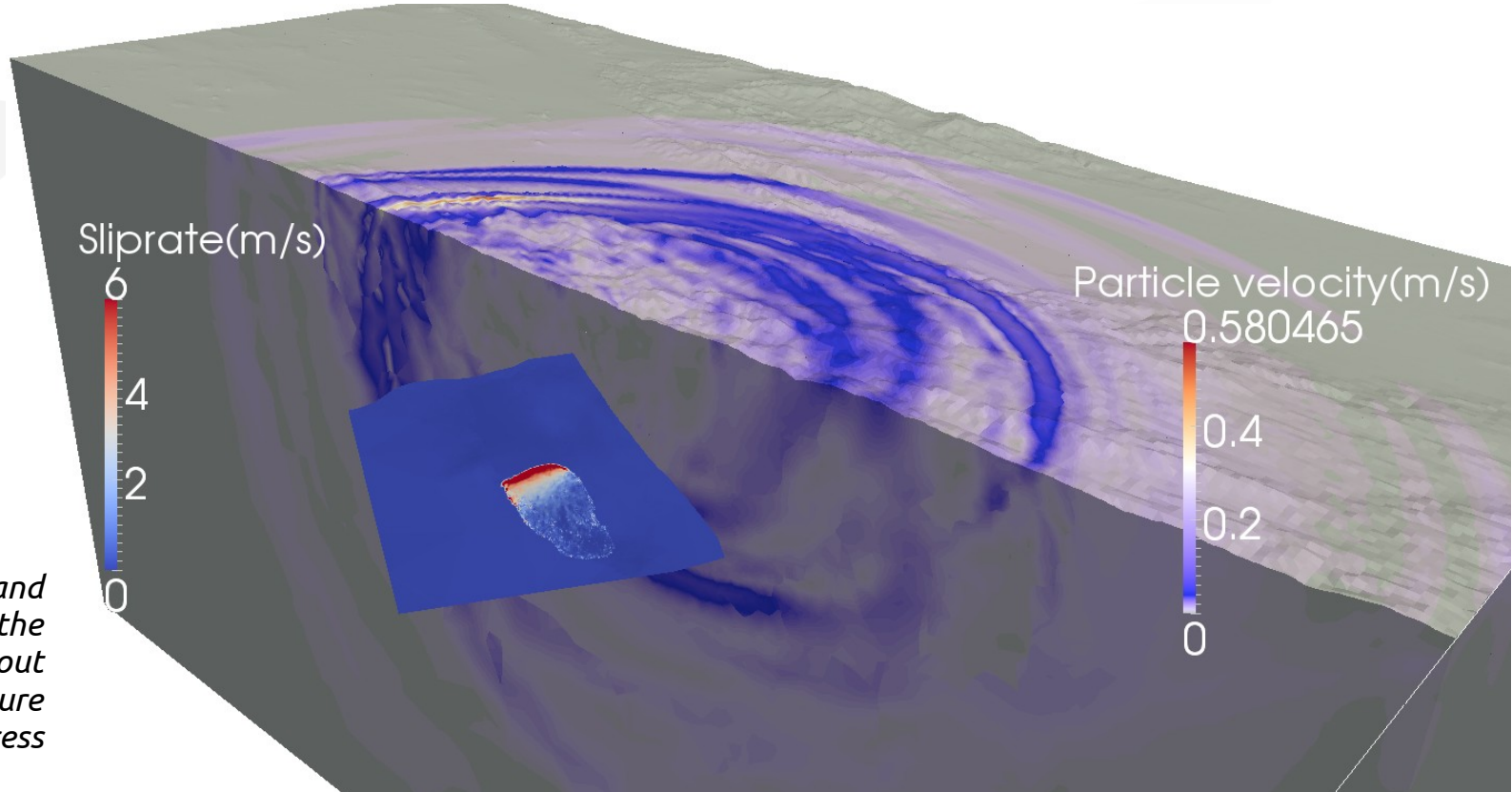

Snapshot of absolute slip rate and emanated seismic wave field on the curved Northridge fault throughout the dynamic earthquake rupture process

Mw 6.7 Northridge earthquake scenario

Normalized velocity seismograms at the two hard-rock SGM stations "SCS" and "NSO" generated with a 1D velocity model for 0.1...1 Hz

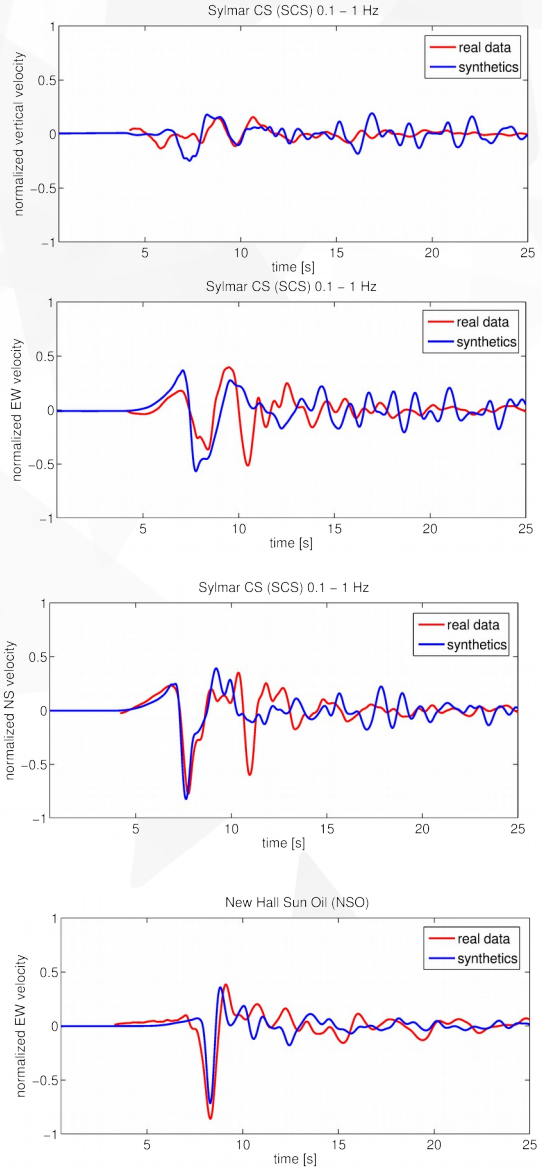

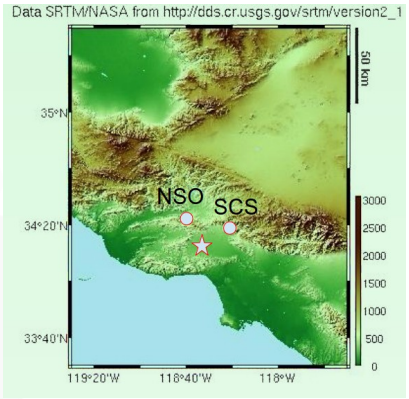

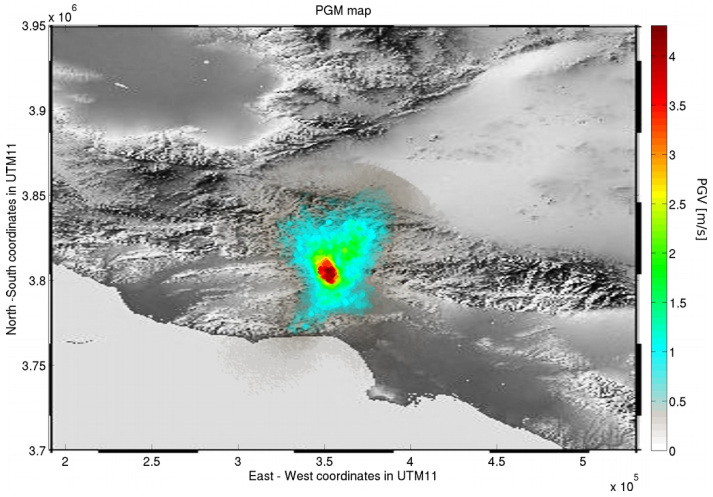

PGV map in a 1D velocity model

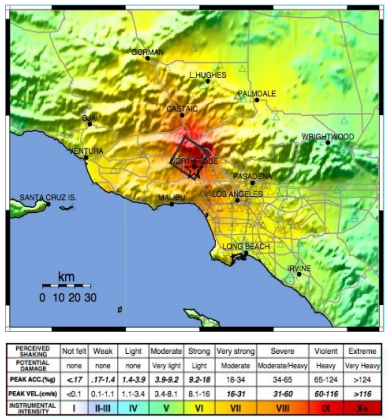

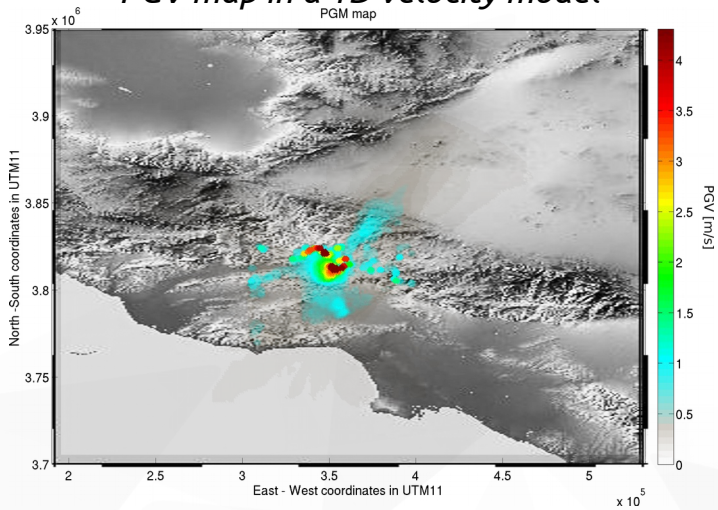

PGV map in a 3D velocity model

- Surprisingly good fit of normalized synthetic waveforms even in 1D velocity model
- Fault geometry and the orientation of the background stress field seem to have major impact on the observed ground motions, as does the regional velocity model

Outlook: Performance enhancements

Current developments:

- Checkpointing

  → checkpoint size: 2.4 GB/node, overhead for writing a checkpoint every 1,000 timesteps is less than 0.5‰

- Optimizing time-to-solution = optimizing energy consumption
- overlap computation and communication (using more effective data layout)

Future developments:

- Local time stepping

  → communication of time-integrated variables (instead of simple ghost cell exchange)

  → more asychronous updates

- CAD and meshing workflow

Towards a community open source package (under BSD3 license)

- Documentation, examples, user interface, first-level user support, ...

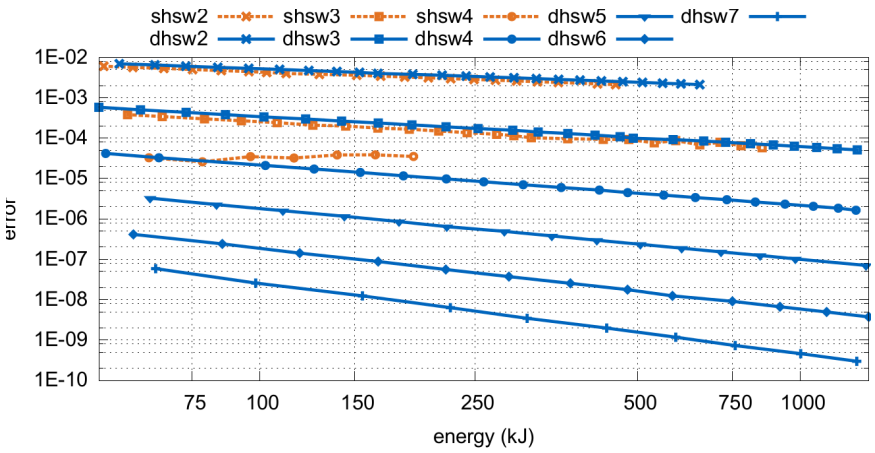

SimModeler Meshing Suite by Simmetrix/Scorec/RPI

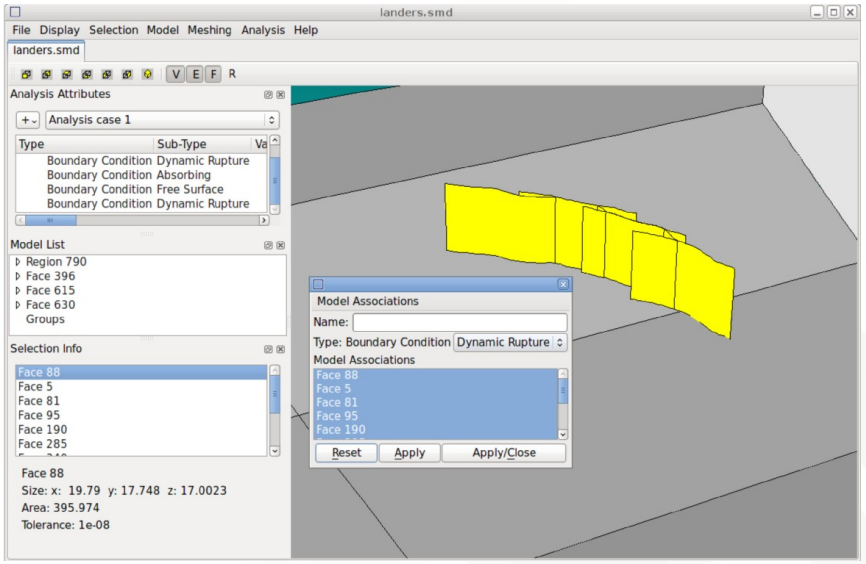

SimModeler Meshing Suite by Simmetrix/Scorec/RPI

Outlook: Tsunamigenic earthquakes

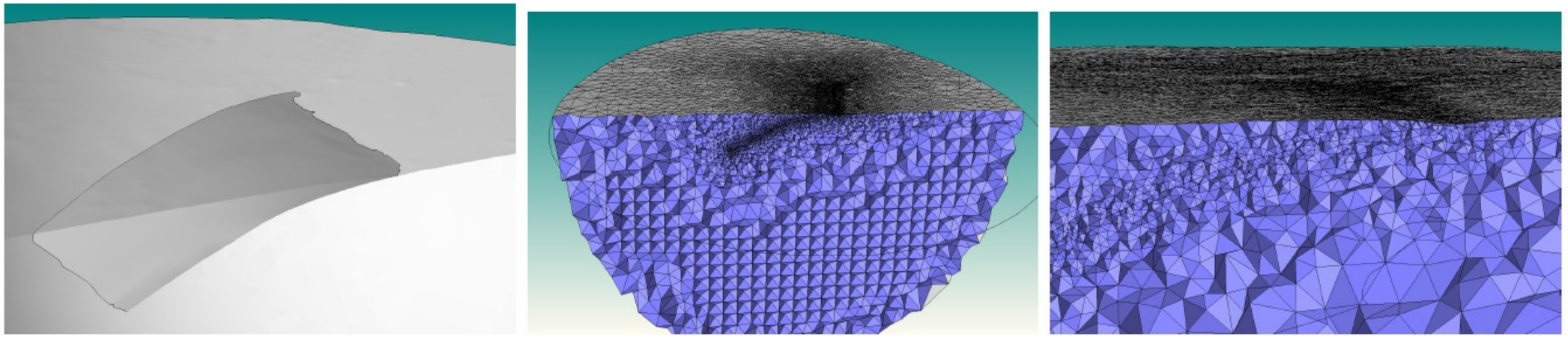

CAD and unstructured mesh generation for the 2011 Tohoku fault segment.

- Local time stepping and mesh optimization to handle challenging 3D subduction zone geometries

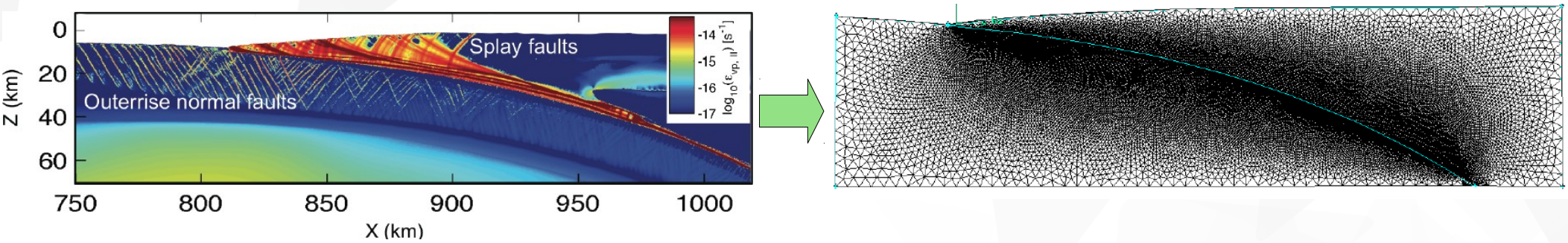

Model geometry, rheology, fault stresses and strengths are imported from the 2D continuum seismo-thermo-mechanical code I2ELVIS (Gerya and Yuen, PEPI, 2007; van Dinter et al., JGR, 2013a,b; van Dinther et al., GRL, 2014)

- Coupling of SeisSol to a geodynamic seismic cycling model to constrain initial conditions

Conclusions

- **Petascale Dynamic Rupture Simulations on modern supercomputers (Tianhe-2, Stampede and SuperMUC)**

- SeisSol enables the study of different representations of complexity which possibly influence the high-frequency content of the seismic wave field with excellent scalability on modern HPC systems

- Fault geometry concurrently with the regional background stress setting is a major influence on rupture dynamics, e.g. resulting in a pulse-like rupture in the Northridge scenario; rupture jumps, branches and slip gaps in the Landers scenario

- Constraints of fault geometry and pre-existing stress and strength state on a fault may stem from observations, experiments or modeling

- Modern numerical methods further our understanding of earthquake source physics, support physic-based ground motion research and add to empirical approaches in seismic hazard analysis

- **SeisSol is on the way to Open Source (BSD-3)**
  Contact me for Beta-Version availability!

Thank you!

gabriel@geophysik.uni-muenchen.de

Visualization